Journal of The Electrochemical Society, 2022 **169** 040551

EDITORS' CHOICE

Editors' Choice—Review—Designing Defects and Diffusion through Substitutions in Metal Halide Solid Electrolytes

Sinclair R. Combs,[1] Paul K. Todd,[2] Prashun Gorai,[2,3] and Annalise E. Maughan[1,2,z]

[1]*Department of Chemistry, Colorado School of Mines, Golden, Colorado 80401, United States of America*
[2]*National Renewable Energy Laboratory, Golden, Colorado 80401, United States of America*
[3]*Metallurgical and Materials Engineering, Colorado School of Mines, Golden, Colorado 80401, United States of America*

Ternary metal halides A_3MX_6, ($A = Li^+$, Na^+; M = trivalent metal; X = halide) are a promising family of solid electrolytes for potential applications in all-solid-state batteries. Recent research efforts have demonstrated that chemical substitution at all three sites is an effective strategy to controlling battery-relevant material properties. The A_3MX_6 family exhibits a wide breadth of structure and anion sublattice types, making it worthwhile to comprehend how chemical substitutions manifest desirable functional properties including ion transport, electrochemical stability, and environmental tolerance. Yet, a cohesive understanding of the materials design principles for these substitutions have not yet been developed. Here, we bring together prior literature focused on chemical substitutions in the A_3MX_6 ternary metal halide solid electrolytes. Using materials chemistry perspectives and principles, we aim to provide insights into the relationships between crystal structure, choice of substituting ions and the extent of substitutions, ionic conductivity, and electrochemical stability. We further present targeted approaches to future substitution studies to enable transformative advances in A_3MX_6 solid electrolytes and all-solid-state batteries.
 [DOI: 10.1149/1945-7111/ac5bad]

Manuscript submitted January 2, 2022; revised manuscript received February 25, 2022. Published April 27, 2022. *This paper is part of the JES Focus Issue on Women in Electrochemistry.*

All-solid-state batteries (ASSBs) are poised to meet the rising demand for high energy density storage technologies. Replacing the liquid electrolyte with a solid-state ion conductor holds several key advantages over current Li-ion battery technologies, including improved mechanical and thermal stability, improved safety, and the potential to improve energy density through use of lithium metal anodes.[1,2] Advancing ASSB technologies is predicated on identifying solid electrolytes (SEs) that simultaneously exhibit high ionic conductivity and good electrochemical stability with desired electrode chemistries.

Ternary alkali metal halides of the general formula A_3MX_6 ($A = Li^+$, Na^+; $M = In^{3+}$, Sc^{3+}, Y^{3+}, Yb^{3+}, Er^{3+}; $X = Cl^-$, Br^-, I^-) have recently gained attention as candidate solid electrolytes for ASSBs. In comparison to popular sulfide-based SEs such as $Li_{10}GeP_2S_{12}$ and the argyrodites Li_6PS_5X (X = halide, pseudohalide), metal halide electrolytes have demonstrated excellent electrochemical stability with high-voltage oxide cathodes and improved stability against lithium metal anodes.[3,4] Further, several members of this material family exhibit improved air and moisture tolerance[5–7] and may be synthesized by low-temperature[8] or solution-phase chemistries and deposited directly onto electrodes.[8,9]

Recent research efforts in the ternary metal halides have focused extensively on using chemical substitutions to achieve high ionic conductivities necessary for practical battery cycling. For example, aliovalent substitution of Zr^{4+} or Hf^{4+} at the trivalent cation site leads to higher ionic conductivities across multiple A_3MX_6 chemistries and structures due to the formation of mobile ion vacancies,[10–15] while isovalent substitution at the M and X sites has been shown to impact moisture tolerance[6] and ion migration pathways.[16–18] Given the relative ease of preparing substituted members of the A_3MX_6 family and the corresponding impact on their functional properties, there is a need for a cohesive set of design principles for how these substitutions influence properties that are relevant for ASSBs.

In this Review, we aim to codify an understanding of how aliovalent and isovalent substitutions at the A, M, and X sites impact the structure, ionic conductivity, and electrochemical stability of ternary metal halide SEs (Fig. 1). Given the breadth of the chemical and structural phase space of this family, we have chosen to focus on ternary metal halides of the A_3MX_6 family for which the A site is occupied by either lithium or sodium ions and in which chemical substitutions have been leveraged as a strategy to modulate electrochemical properties for SE applications. We anticipate that the design principles and composition-structure-property relationships derived from this smaller subset of the alkali metal halide family may be readily extended to other ternary metal halide compositions and structures. For review of the broader ternary metal halide family, the reader is referred to the works of Li et al.[19] and Liang et al.[20]

A Brief Primer on Ion Conduction Mechanisms in the Solid State

In the crystalline solid state, ionic conductivity proceeds through a thermally-activated process in which mobile ions hop between neighboring sites within the periodic structure along a minimum energy pathway.[21–23] The energy barrier associated with this hopping process is known as the migration barrier (E_m) and is dictated by several factors, including the volume of the migration pathways and the electrostatic interactions between the mobile ions and the surrounding host structure. Chemical substitutions can be used as a strategy to lower the migration barrier by expanding the size of the physical bottlenecks or by moderating the Coulomb interactions between the mobile ions and the surrounding host structure. In addition to the migration barrier, the bulk ionic conductivity is also dependent upon the concentration of defects (vacancies, interstitials, partial occupancies) that mediate diffusion. Aliovalent substitutions provide a method to modulate the concentration of mobile ion vacancies, and the energy associated with forming mobile defects due to these substitutions is characterized by the trapping energy (E_t). Overall, ionic conductivity is governed by the total activation barrier, E_A, which contains contributions from both E_m and E_t. We note that the effects of structure tuning and substitution on E_m and E_t are highly interdependent and are not easily deconvoluted.

The A_3MX_6 Family

Structure types.—The A_3MX_6 family encompasses a broad compositional and structural phase space. For the solid electrolytes in which $A = Li^+$ or Na^+, several distinct structure types are observed and are shown in Fig. 2. A common structural theme among the A_3MX_6 family is the local coordination environment of

[z]E-mail: amaughan@mines.edu

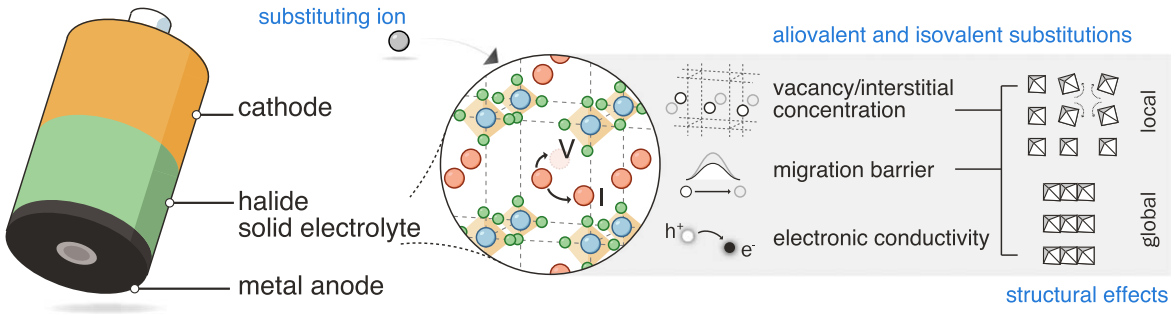

Figure 1. Aliovalent and isovalent substitutions in solid electrolytes affect the mobile ion vacancy and interstitial concentrations, migration barrier of the diffusing mobile ion, and electronic conductivity. Substitutions induce local, and in some cases, global structural changes that affect mobile ion defect concentrations and migration barriers.

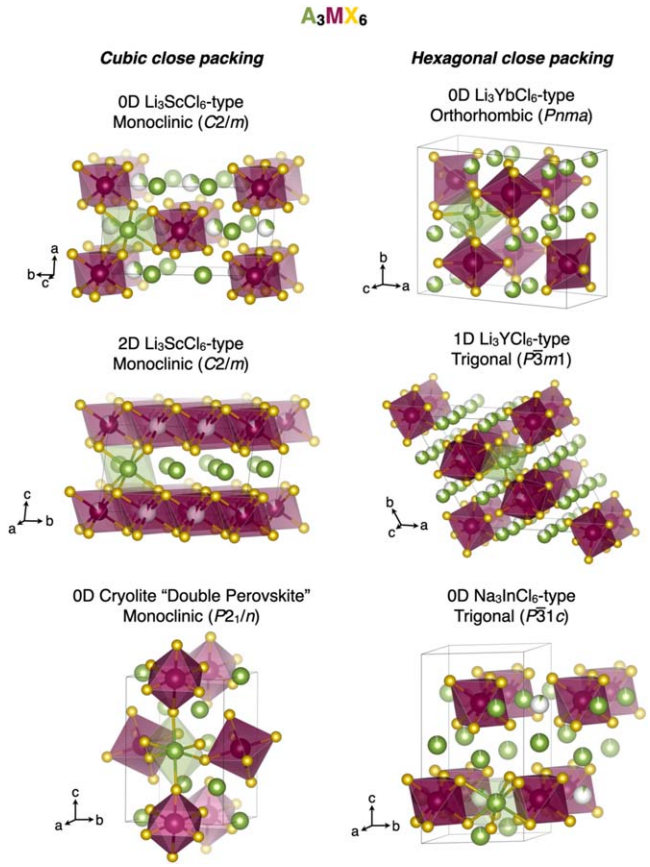

Figure 2. Structure types commonly found in the A_3MX_6 solid electrolytes. Alkali ions (A) are green, metals (M) are magenta, and halide (X) are gold. The structure types are divided into those that adopt cubic close-packed (ccp) and hexagonal close-packed (hcp) halide sublattices. A single AX_6 octahedron (green) is shown to highlight the octahedral coordination environment of the mobile alkali ions.

the A- and M-site cations. Both the alkali ions and trivalent metal ions occupy octahedral sites and the different structure types are distinguished by close-packing of the halide sublattice. Cubic close-packed (ccp) structures are found for the 0D and 2D variants of the Li_3ScCl_6 structure type. We note that the 0D and 2D variants of the Li_3ScCl_6 structure type are effectively identical and are only distinguished by ordering of the A and M cationic sublattice. A distorted ccp sublattice is also found in the cryolite "double perovskite" structure type that is typically observed for larger alkali ions. The ccp halide sublattices are often found for materials in which the radius of the M site is small relative to the size of the coordinating halides.[20] Alternatively, structure types with hexagonal close-packed (hcp) anion sublattices are often found in the A_3MX_6 family for larger M-site ions. These structure types include 0D orthorhombic Li_3YbCl_6-type (*Pnma*), 1D trigonal Li_3YCl_6-type ($P\bar{3}m1$), and 0D trigonal Na_3InCl_6-type ($P\bar{3}1c$). An in-depth discussion of how the combination of A, M, and X sites favors particular structural topologies has been presented elsewhere.[19,20,24] A compiled table of A_3MX_6 structure types and phases relevant to the remainder of this Review are presented in Table I.

Ion migration pathways.—Packing of the halide sublattice in the A_3MX_6 family dictates the geometry of the ion migration pathways and the coordination environment of the interstitial sites through which mobile ions migrate.[46] In ccp structure types, ion transport proceeds through an oct-tet-oct pathway, in which mobile ions hop between neighboring octahedral sites through a tetrahedral interstitial (Fig. 3a). In contrast, ion migration in hcp structures occurs through an oct-oct-tet-oct pathway; mobile ions migrate through the shared triangular face of two AX_6 octahedra and then through the neighboring tetrahedral interstitial site (Fig. 3b). We anticipate that the differences in migration pathways will affect how aliovalent and isovalent substitutions impact ion transport in these materials by impacting the migration barrier as well as the formation of vacancies and interstitials. The specific effects will be discussed in greater detail in the respective sections, below.

Aliovalent Substitution

Aliovalent substitution involves replacing ions in the host structure of the SE with ions of differing formal charge and has been widely employed to enhance ionic conductivity in the A_3MX_6 family as well as other SEs. The enhancement in ionic conductivity is brought about by two distinct local effects: (a) creation of vacancies and interstitials, and (b) modification of the energy landscape in the diffusion channels in a way that lowers the migration barrier.

The increase in the mobile ion vacancy (or interstitial) concentration is often rationalized by considering that the additional charge due to aliovalent substitution is compensated by the formation of charged vacancies or interstitials. This ignores the potential for electronic compensation, which is only valid for wide-bandgap materials; these effects will be discussed in greater detail in the Electrochemical Stability section.

We can understand the thermodynamic origin of the increase (or decrease) in ionic conductivity by considering how the formation energy of native defects in an SE change in response to aliovalent doping. Defect formation energy ($\Delta E_{D,q}$) can be determined from first-principles calculations,[47–49] where D denotes the defect type (*e.g.*, lithium vacancy V_{Li}) and q is the charge state (*e.g.*, V_{Li}^{-1}). Computed $\Delta E_{D,q}$ are typically presented in the form of a "defect diagram", which is schematically shown in Fig. 4. $\Delta E_{D,q}$ of different types of defects are plotted as a function of the Fermi energy (E_F), which is referenced to the valence band maximum (VBM). For each

Table I. A_3MX_6 solid electrolytes and structure types discussed in this Review. Dashes indicate that the composition has not been reported in the A_3MX_6 stoichiometry.

Material	Structure Type	Space group	Reference
Li_3AlF_6	$Zn_4Ta_2O_9$	$C2/c$	25
Li_3AlCl_6 [a)]	1D Li_3YCl_6	$P\bar{3}m1$	26
Li_3AlBr_6	—	—	—
Li_3AlI_6	—	—	—
Li_3ScF_6	filled Na_2InCl_6	$P\bar{3}1c$	27
Li_3ScCl_6	0D Li_3ScCl_6	$C2/m$	28, 29
Li_3ScBr_6	0D Li_3ScCl_6	$C2/m$	30
Li_3ScI_6 [a)]	Li_3LaI_6	$C2$	31
Li_3InF_6	—	$P2_1/m$	32
Li_3InCl_6	2D Li_3ScCl_6	$C2/m$	5, 33
Li_3InBr_6	2D Li_3ScCl_6	$C2/m$	34
Li_3InI_6	—	—	—
Li_3YbF_6	—	—	—
Li_3YbCl_6	0D Li_3YbCl_6	$Pnma$	35
Li_3YbBr_6	2D Li_3ScCl_6	$C2/m$	28
Li_3YbI_6	—	—	—
Li_3ErF_6	—	—	—
Li_3ErCl_6	1D Li_3YCl_6	$P\bar{3}m1$	35
Li_3ErBr_6	2D Li_3ScCl_6	$C2/m$	28
Li_3ErI_6	2D Li_3ScCl_6	$C2/m$	36
Li_3YF_6	—	—	—
Li_3YCl_6	1D Li_3YCl_6	$P\bar{3}m1$	35, 37
Li_3YBr_6	2D Li_3ScCl_6	$C2/m$	28, 37
Li_3YI_6 [a)]	Li_3LaI_6	$C2$	31
Na_3AlF_6	Cryolite	$P2_1/n$	38
Na_3AlCl_6	—	—	—
Na_3AlBr_6	—	—	—
Na_3AlI_6	—	—	—
Na_3ScF_6	Cryolite	$P2_1/n$	39
Na_3ScCl_6	Cryolite	$P2_1/n$	39
Na_3ScBr_6	—	—	—
Na_3ScI_6	—	—	—
Na_3InF_6	0D Li_3ScCl_6	$C2/m$	40
Na_3InCl_6	0D Na_3InCl_6	$P\bar{3}1c$	41
Na_3InBr_6	—	—	—
Na_3InI_6	—	—	—
Na_3YbF_6	—	—	—
Na_3YbCl_6	Cryolite	$P2_1/n$	42
Na_3YbBr_6	Cryolite	$P2_1/n$	43
Na_3YbI_6	—	—	—
Na_3ErF_6	—	—	—
Na_3ErCl_6	Cryolite	$P2_1/n$	10
Na_3ErBr_6	Cryolite	$P2_1/n$	43
Na_3ErI_6	—	—	—
Na_3YF_6	—	—	—
Na_3YCl_6	Cryolite	$P2_1/n$	44
Na_3YBr_6	Cryolite	$P2_1/n$	43
Na_3YI_6 [a)]	2D Li_3ScCl_6	$P2_1/n$	45

a) Computationally predicted.

defect, the slope represents the charge state at a given E_F such that defects with positive q are donor-like and those with negative q are acceptor-like.

For the sake of simplicity, let us consider a SE with negatively-charged Li vacancies (V_{Li}^{-1}) and a positively-charged native donor defect, as shown in Fig. 4a. The equilibrium Fermi energy ($E_{F,eq}$), denoted by the vertical dashed line, is obtained by self-consistently solving the condition of charge neutrality between the positive

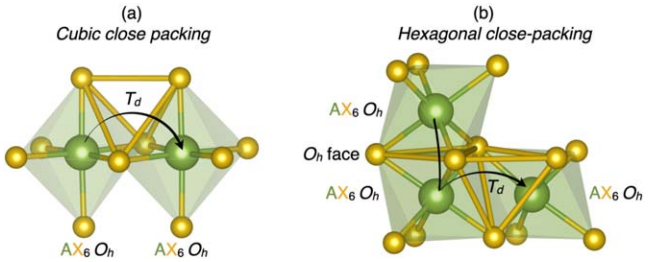

Figure 3. Local ion hopping pathways identified for structures with (a) cubic close-packed and (b) hexagonal close-packed anion structures. Green ions are mobile alkali ions and gold are halides. We have drawn halide-halide bonds where relevant to highlight the geometry of the migration pathways.

($+q$ defects, holes) and the negative ($-q$ defects, electrons) charges. For a more detailed description, see Refs. 47 and 48. It is the formation energy of the defects at $E_{F,eq}$ that is relevant; in wide-gap materials such as SEs, $E_{F,eq}$ generally lies close to the intersection of the lines representing the lowest-energy acceptor and donor defects.

When a sufficiently soluble donor aliovalent dopant is introduced in the SE, it creates a donor state with low $\Delta E_{D,q}$ (Fig. 4b). If $\Delta E_{D,q}$ of the donor dopant is lower than the lowest native donor defect, then $E_{F,eq}$ shifts toward the conduction band concomitantly lowering the formation energy of V_{Li}. At the same time, excess electrons are generated because the $E_{F,eq}$ now lies closer to the conduction band. It is worth noting that the excess charge created by the donor alivovalent dopant is not completely compensated by the formation of excess V_{Li}; excess electrons are generated, the concentration of which can be relatively low compared to the ionic conductivity depending on the position of $E_{F,eq}$ relative the CBM. Whether the excess electrons (or holes) will contribute to electronic conductivity depends on the shallow vs. deep nature of the defects. Nevertheless, the simplified scenario presented in Fig. 4 provides a more detailed thermodynamic picture of the effect of aliovalent doping and its impact on the defect energetics.

M-*site aliovalent substitution.*—Aliovalent M-site substitution has recently been employed as a strategy to achieve high ionic conductivities across several members of the A_3MX_6 family. Several closely-related properties impact ion migration. Introduction of higher-valency ions (*e.g.*, Zr^{4+}, Hf^{4+}) is compensated by mobile ion vacancies, which promote fast ion conduction by providing available sites for mobile cations to jump to during their migration process.[50] Beyond tuning the mobile ion carrier density, M-site substitution can also impact ion transport through changes to the underlying crystal structure. Changes in bulk crystal structure and rearrangement of the close-packed anion sublattice upon substitution in heterostructural systems modifies the migration pathways and conduction mechanisms. In isostructural or "alloy" substitution systems where substitution does not induce a change in crystal structure, introduction of extrinsic ions of differing size can expand or contract the migration pathways to affect the migration barrier or impact the local coordination environment surrounding mobile ions. Thus far, tetravalent zirconium and hafnium are the most commonly employed choice for aliovalent substitutions at the M^{3+} site. Both ions are found almost exclusively in the 4+ oxidation state and therefore offer good redox stability[51,52] and the ionic radii ($r(Zr^{4+}) = 72$ pm, $r(Hf^{4+}) = 71$ pm)[53] are most similar to that of common M^{3+} ions compared to other smaller tetravalent cations. While M-site aliovalent substitution is a promising strategy for improving ionic conductivity in ternary metal halides, the relationships between the choice of substituting ion, extent of substitution, structure, ion migration pathways, and ionic conductivity are currently not well-understood. Here, we highlight existing studies of M-site aliovalent substitution in an effort to develop an understanding of the complex interplay between structure, substitution, and ion transport.

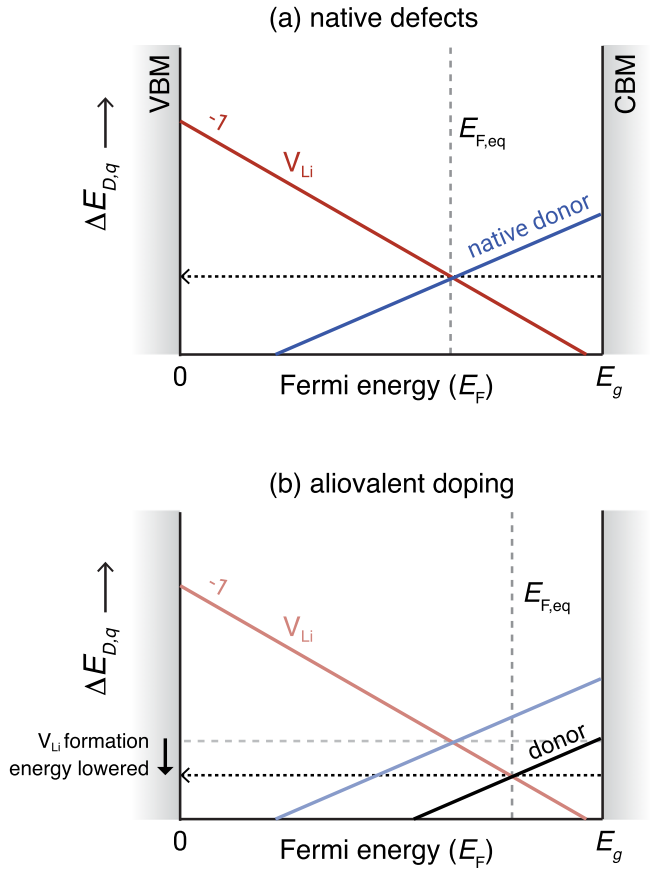

Figure 4. Schematic of a defect diagram where the calculated formation energy of a defect ($\Delta E_{D,q}$) is plotted as function of the Fermi energy (E_F). (a) Formation energy of native defects in a solid electrolyte, including the acceptor Li vacancy (V_{Li}) and a native donor. The E_F is pinned close to the intersection between the native acceptor and donor defects; $\Delta E_{D,q}$ at the equilibrium Fermi energy $E_{F,eq}$ is relevant. (b) Formation energy of a substituted extrinsic donor (*e.g.*, Zr^{4+} at *M* site in A_3MX_6) relative to the native defects. When the donor substitution is favorable, $E_{F,eq}$ is shifted toward the conduction band such that $\Delta E_{D,q}$ of Li vacancies is lowered. Consequently, V_{Li} concentration and Li-ion conductivity increases.

Aliovalent substitution often induces a change in the crystal structure and subsequently impacts ion transport properties. Figure 5 illustrates the trends in ionic conductivity and activation barrier for *M*-site aliovalent substitution in several Li_3MCl_6 materials, and are grouped by the crystal structures that are observed with aliovalent substitution. The structural changes upon aliovalent substitution in $Li_{3-x}Yb_{1-x}M'_xCl_6$ ($M' = Zr^{4+}$, Hf^{4+}) are particularly intriguing, as the observed structures depend on the preparation temperature. When prepared at low temperatures ($T = 350$ °C–400 °C), Li_3YbCl_6 adopts the trigonal Li_3YCl_6 structure type ($P\bar{3}m1$) with an hcp anion sublattice (Fig. 5a). Upon substitution, the ionic conductivities increase by approximately an order of magnitude from 10^{-5} to 10^{-4} S cm^{-1} for $x = 0$ to $x = 0.1$. At 20% substitution, the structure changes from the trigonal structure type to the layered 2D Li_3ScCl_6 structure type ($C2/m$) characterized by the lessdense ccp anion sublattice.[13,14] At this point, the conductivity plateaus and then decreases with further aliovalent substitution. Distinct structural behavior of $Li_{3-x}Yb_{1-x}M'_xCl_6$ is observed when the materials are prepared at higher temperatures ($T = 550$ °C–600 °C), as shown in Fig. 5b.[13,14] The unsubstituted Li_3YbCl_6 adopts an orthorhombic structure (*Pnma* I, hcp) and transitions to a distorted orthorhombic structure (*Pnma* II, hcp) upon ~25% substitution of Zr^{4+}/Hf^{4+}. Similarly to the materials prepared at lower temperatures, the conductivity increases rapidly for $x = 0$ to $x = 0.25$ and then begins to decrease with further substitution. The ability to direct the formation of either ccp or hcp structures through judicious choice of preparation conditions provides an exciting avenue to design substituted metal halide SEs with desirable structure types.

Li_3YCl_6 and Li_3ErCl_6 exhibit similar structural behavior upon Zr^{4+} substitution (Fig. 5c).[54] Both unsubstituted materials adopt the trigonal Li_3YCl_6 structure type ($P\bar{3}1$, hcp). The trigonal structure is retained for Zr^{4+} substitution up to 10%, at which point a mixed phase region is observed from $x = 0.1$ to $x = 0.4$ for both materials. Above $x = 0.4$, the substituted structures adopt the distorted orthorhombic structure (*Pnma* II) familiar to the high-temperature polymorphs of $Li_{3-x}Yb_{1-x}M'_xCl_6$ (Fig. 5a,b).[13,14] It is interesting to note that the general trends in ionic conductivity and activation barrier are fairly conserved for heterostructural substitutions across the compositional and structural variants shown in Fig. 5, suggesting that the underlying migration pathways are impacted similarly by aliovalent substitution in these heterostructural systems.

Both zirconium and hafnium exhibit low solubility into the host structures of Li_3YbCl_6, Li_3YCl_6, and Li_3ErCl_6 before bulk changes in the crystal structure are observed. We attribute the low solubility limits of Zr^{4+} to the disparate structures of the Li_3MCl_6 and Li_2ZrCl_6 endmembers. Li_2ZrCl_6 adopts a monoclinic structure ($C2/m$) with a cubic close-packed anion sublattice that is nearly identical to the layered Li_3ScCl_6 structure type. In contrast, the Li_3MCl_6 materials presented in Fig. 5 adopt structures with hexagonal close-packed anion sublattices. We propose that competition between ccp and hcp sublattices is responsible for driving the phase transitions at low concentrations of Zr^{4+}. While we do not have structural data for Li_2HfCl_6, the similar sizes and chemistries of Zr^{4+} and Hf^{4+} presumably favor the formation of similar structures. Beyond our speculation, a fundamental understanding the driving forces between these structural changes is necessary to exploit phase transitions as a design principle in the A_3MX_6 family.

In contrast to the heterostructural systems discussed above, Zr^{4+} substitution in Li_3InCl_6 does not induce changes in the crystal structure or anion close-packing. Li_3InCl_6 adopts the layered 2D Li_3ScCl_6 structure type ($C2/m$, ccp) with alternating layers of $InCl_6$ and $LiCl_6$ octahedra (Fig. 2). Upon Zr^{4+} substitution, the $C2/m$ ccp structure is preserved across the solid solution series between Li_3InCl_6 and Li_2ZrCl_6, though Helm et al. note diminished crystallinity above $x = 0.5$.[12,15] The ability to alloy Li_3InCl_6 and Li_2ZrCl_6 presumably stems from the fact that the endmembers are isostructural; both adopt cubic-close packed structures ($C2/m$) with layered slabs of MCl_6 and $LiCl_6$ octahedra.[55,56] Therefore, the influence of Zr^{4+} substitution on the ionic conductivity in $Li_{3-x}In_{1-x}Zr_xCl_6$ will arise from a combination of Li^+ vacancies and changes in the volume of the migration pathways rather than changes in crystal structure or migration pathways.

Zr^{4+} substitution generally appears to increase the ionic conductivity of $Li_{3-x}In_{1-x}Zr_xCl_6$ (Fig. 6a).[12,15] In the study by Helm et al., the ionic conductivity increases monotonically from 4.7×10^{-4} S cm^{-1} for Li_3InCl_6 and reaches a maximum of 1.2×10^{-3} S cm^{-1} at $x = 0.4$.[15] Luo et al. identified a maximum ionic conductivity at $x = 0.1$, though it is difficult to identify a trend in the ionic conductivities with Zr^{4+} concentration.[12] Rather, the ionic conductivities reported by Luo et al. appear to trend roughly with the unit cell volumes in this study. This result is distinct from Helm et al. which demonstrated a linear decrease in lattice parameters with increasing Zr^{4+}.[15] The differences observed between the studies by Helm et al. and Luo et al. suggest that the structures and ionic conductivities in these materials are highly sensitive to preparation and measurement methods. Interestingly, both Helm et al. and Luo et al. identified a substantial increase in cation disorder upon Zr^{4+} substitution. In Li_3InCl_6, the $InCl_6$ and $LiCl_6$ octahedra are separated into distinct slabs. Upon substitution, the Li^+ ions begin occupying the cation sites within both layers and effectively enable diffusion along the layer stacking direction. The reorganization of the lithium substructure and newly-formed 3D migration

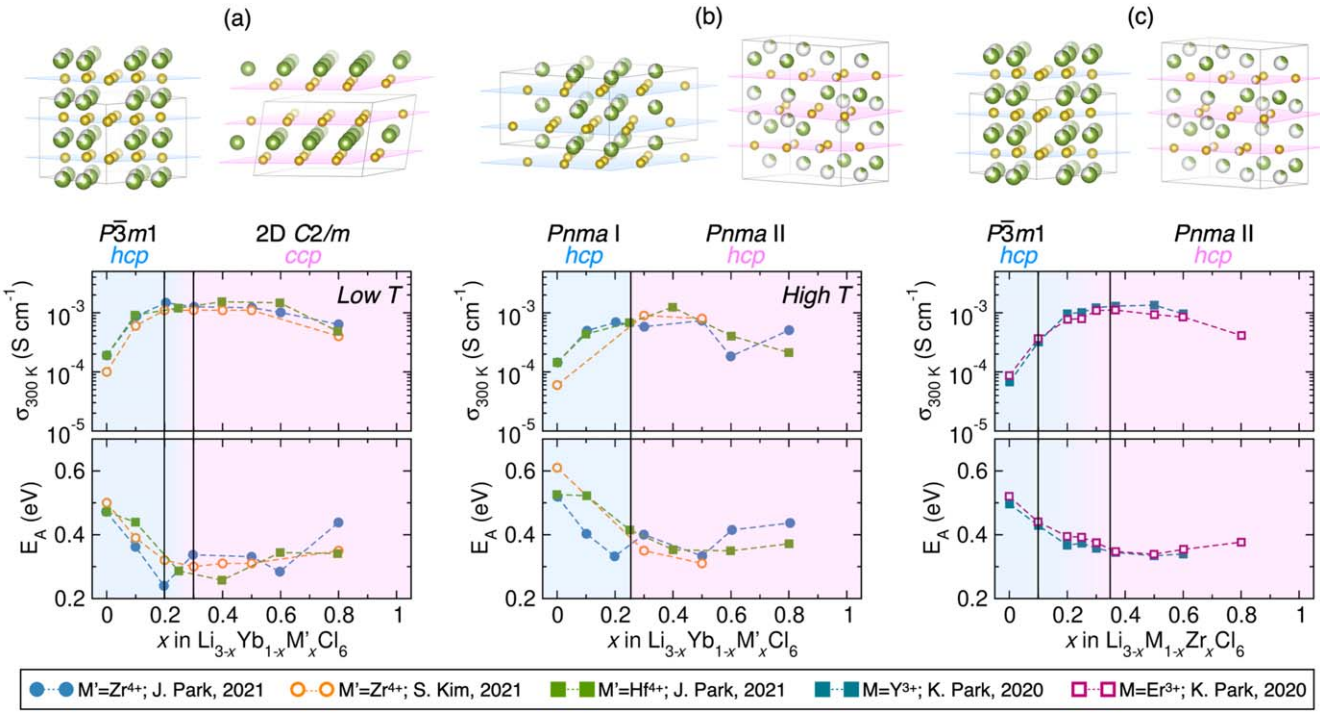

Figure 5. Relationships between substitution amount, room-temperature ionic conductivity (σ_{300K}), and activation barrier (E_A) for members of the A_3MX_6 family for which substitution is accompanied by a structure change. The blue and pink shaded regions highlight the concentration ranges of the observed structures; gradients indicate mixed phase regions. The close-packed planes of the halide sublattices are shown in the structural representations above. *M*-site aliovalent substitutions for $Li_{3-x}Yb_{1-x}M'_xCl_6$ ($M' = Zr^{4+}$, Hf^{4+}) prepared at (a) low temperatures (350 °C–400 °C) and (b) high temperatures (550 °C–600 °C).[13,14] In (c), Zr^{4+} substitution in Li_3YCl_6 and Li_3ErCl_6 are shown.[54]

pathways combined with mobile ion vacancies is proposed to enable higher ionic conductivities in $Li_{3-x}In_{1-x}Zr_xCl_6$. Although it is challenging to separate the impacts of crystal structure, vacancy formation, and bottleneck size on ionic conductivity, the ability to retain the cubic close-packed sublattice while restructuring the mobile ion migration pathways presents an exciting opportunity to couple these effects to design A_3MX_6 materials with beneficial ion transport properties.

The impacts of aliovalent *M*-site substitution are also readily extended to the sodium-based analogs. As shown in Fig. 6b, substitution of Zr^{4+} in Na_3YCl_6[11] and Na_3ErCl_6[10] is accompanied by a nearly five orders-of-magnitude increase in the ionic conductivity from $\sim 10^{-9}$ S cm^{-1} to $\sim 10^{-5}$ S cm^{-1}. Similarly to the example of $Li_{3-x}In_{1-x}Zr_xCl_6$ (Fig. 6a), both Na_3YCl_6 and Na_3ErCl_6 adopt structures with distorted ccp halide sublattices (cryolite, $P2_1/n$) and the crystal structures are conserved up to ~85% Zr^{4+}, at which point mixed phases and the Na_2ZrCl_6 endmember (trigonal, $P\bar{3}m1$) are observed.[57] The ability to alloy ccp structures of Na_3YCl_6 and Na_3ErCl_6 with the hcp structure of Na_2ZrCl_6 is intriguing in the context of the substantial structural changes observed in the Li-based systems that exhibit disparate anion sublattices between the endmembers. For example, only 20% Zr^{4+} is permitted to substitute in Li_3YbCl_6 (hcp) before a bulk structural change to the structure of Li_2ZrCl_6 (ccp) (Fig. 5a). This observation suggests that either the distorted ccp sublattice of the cryolite structure type is more amenable to these substitutions or that the larger size of the Na^+ alkali ion stabilizes the ccp structure across a broader compositional space. The ability to preserve the less-dense ccp structure while simultaneously tuning the concentration of mobile ion vacancies therefore presents a materials design strategy for achieving high ionic conductivities in other members of this SE family.

We can attribute the trends in Na-ion conductivities with Zr^{4+} substitution to several conflating factors. Schlem et al. noted that the volume of the octahedral Na^+ sites in $Na_{3-x}Er_{1-x}Zr_xCl_6$ remains fairly constant for $x = 0$–0.6 despite an overall contraction of the unit cell.[10] This observation suggests that the volume of the Na^+ migration pathways is initially unchanged with Zr^{4+} substitution, and thus the rapid increase in ionic conductivity from $x = 0$–0.2 is likely enabled by the formation of Na^+ vacancies. At higher concentrations, the increasing number of vacancies competes with shrinking unit cell volume and the electrostatic stabilization from reduced Na–Na interactions, resulting in a decrease in ionic conductivity beyond $x = 0.6$. These observations suggest a complex interplay of factors that contribute to the observed Na-ion transport properties.

The impacts of aliovalent *M*-site substitution on ion conduction are, in a large part, based on the presence of a cubic close-packed or hexagonal close-packed sublattice structure. This is exemplified by comparing the ionic conductivities of unsubstituted members of the Li_3MX_6 family. As shown in Fig. 6, the ionic conductivity of Li_3InCl_6 before substitution is substantially higher than other members of the Li_3MCl_6 family; the unsubstituted materials presented in Fig. 5 tend to exhibit ionic conductivities on the order of 10^{-5}–10^{-4} S cm^{-1}, while Li_3InCl_6 exhibits an ionic conductivity of 4.7×10^{-4} S cm^{-1}.[15] This observation can be rationalized by considering the close-packing motifs of the anion sublattices; the lower packing density of the ccp Li_3InCl_6 structure is conducive to higher ionic conductivities than the hcp structures types adopted by the materials presented in Fig. 5.

Close-packing of the anion sublattice further dictates the migration pathways and the subsequent impact of mobile ion vacancies on ion transport. As shown in Fig. 3, ion migration in ccp structures proceeds through an oct-tet-oct interstitial pathway, while ion migration in hcp structures proceeds through oct-oct-tet-oct pathway. We hypothesize that mobile ion vacancies will more strongly impact ion transport in hcp structures compared to ccp structures. In hcp structures, the mobile ions must move between two adjacent octahedra through the direct oct-oct part of the pathway without an intermediate interstitial site (Fig. 3b). As such, we hypothesize that introducing a mobile ion vacancy at the octahedral sites would lower the migration barrier for this part of the pathway.[21]

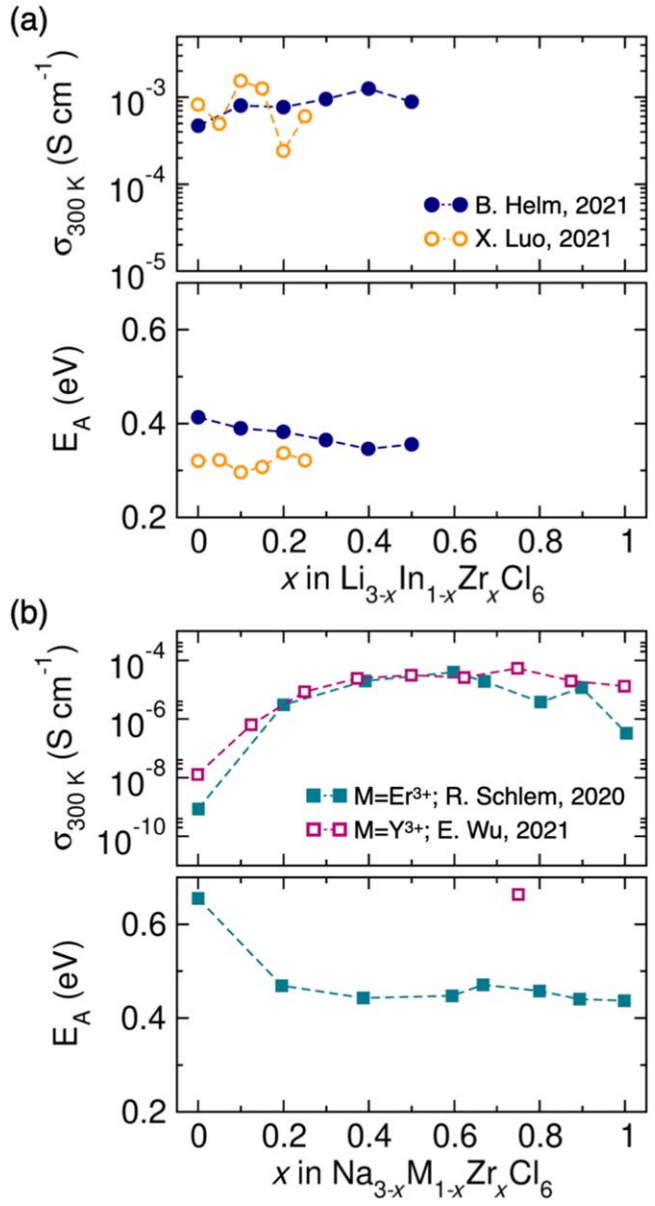

Figure 6. Impact of Zr^{4+} *M*-site aliovalent substitution in cubic-close packed structures (a) Li_3InCl_6[12,15] and (b) Na_3MCl_6 ($M = Y^{3+}$, Er^{3+})[10,11] on room temperature ionic conductivity (σ_{300K}) and activation barrier (E_A). The cubic close-packed anion sublattice is preserved across the substitution range.

In contrast, the migration pathway for ccp structures involves an interstitial mechanism (oct-tet-oct) that we hypothesize is less strongly impacted by the presence of mobile ion vacancies. This hypothesis is supported by the observed impact of mobile ion vacancies on the ionic conductivity in hcp vs ccp structures; in hcp structures (Fig. 5), introduction of lithium ion vacancies is accompanied by an order of magnitude increase in ionic conductivity for even 10% substitution. Conversely, the increase in ionic conductivity for 10% Zr^{4+} substitution in Li_3InCl_6 is far less pronounced.

While *M*-site aliovalent substitutions have focused primarily on higher-valency ions to introduce mobile ion vacancies as a strategy to improve ionic conductivity, there have been a small number of studies focused on substitution of divalent ions at the *M*-site. In contrast to Zr^{4+}/Hf^{4+} substitutions that are compensated by mobile ion vacancies, introducing divalent ions at the *M*-site would be compensated by filling mobile ion vacancies or by excess holes as electronic carriers. Thus, they are not anticipated to be a desirable substitution for improving charge transport or electrochemical stability in the A_3MX_6 SEs. This is exemplified in a study by Tomita et al., which demonstrated that substitution of Zn^{2+}, Co^{2+}, and Fe^{2+} in Li_3InBr_6 was accompanied by a decrease in ionic conductivity in the superionic phase.[16] The authors attributed this observation to compensation by excess Li^+ ions. Interestingly, a computational study by Wan and Ciucci suggested that Sr^{2+} substitution in $Li_{3+x}Y_{1-x}Sr_xCl_6$ lowers the activation barrier for Li-ion conductivity despite the excess mobile ions.[58] This observation can be explained by the larger size of Sr^{2+} compared to Y^{3+}, which expands the physical volume of the ion migration pathways. We also note that divalent ions could feasibly substitute on either the *A* site *or* the *M* site with little discrimination (as discussed in more detail in the following section). As these substitutions will have distinct compensation mechanisms, further studies are necessary to understand the preferred substitution sites within the structure and how divalent ion substitution dictates ion transport properties in these materials. Overall, *M*-site substitution studies have revealed that this type of material modification is beneficial to the ionic conductivity via generation of additional mobile ion vacancies that aid conduction mechanisms. In heterostructural systems, induced phase transitions alter the structure to more favorable anion sublattice types that are beneficial to ion migration pathways.

A-*site aliovalent substitution.*—Aliovalent substitution at the *A* site presents another strategy to modulate the vacancy concentration of mobile ions to impact ion transport. Divalent alkali earth (*AE*) ions are a natural choice for substitution at the *A* site and may be compensated by mobile ion vacancies according to the chemical formula $A_{3-2x}(AE)_xMX_6$. This is exemplified by studies by Tomita et al. which demonstrated systematic substitution of the alkali earth series ($Mg^{2+} \rightarrow Ca^{2+} \rightarrow Sr^{2+} \rightarrow Ba^{2+}$) in the superionic phase of $Li_{3-2x}(AE)_xInBr_6$.[34,59,60] In the superionic phase ($T \geqslant 314$ K), Li_3InBr_6 adopts the layered monoclinic structure familiar to Li_3InCl_6 with 2D conduction lithium-ion migration pathways between the $InBr_6$ sheets (Fig. 7a). Despite the increase in Li^+ vacancies upon substitution of the alkali earth ions ($AE = Mg^{2+}$, Ca^{2+}, Sr^{2+}), the lithium ion conductivity decreases, as shown in Fig. 7b.[60] Interestingly, the decrease in ionic conductivity with alkali earth substitution in $Li_{3-2x}(AE)_xInBr_6$ is in direct contrast to recent studies of aliovalent Ca^{2+} substitution in the halide argyrodite $Li_{6-2x}Ca_xPS_5Cl$, in which Ca^{2+} substitution yielded higher lithium ion conductivities.[61,62] One hypothesis for the reduced ionic conductivities in $Li_{3-2x}(AE)_xInBr_6$ is that the *AE* ions are not substituting at the *A* site but rather occupy the trivalent *M* site. In this scenario, the excess charge could be compensated by excess lithium ions that leads to lower ionic conductivities. Alternatively, in the scenario where the *AE* ions are replacing Li^+ ions, the differences in the structural topologies between the layered Li_3InBr_6 and cubic argyrodite $Li_{6-2x}Ca_xPS_5Cl$ may be responsible for how *AE* substitution influences ion conduction. We hypothesize that the layered structure of Li_3InBr_6 may restrict the available lithium ion migration pathways such that immobile alkali earth ions disrupt the migration pathways for lithium ions despite the larger number of mobile ion vacancies. In contrast, the 3D migration pathways available in the argyrodite structure may provide a larger number of energy-equivalent sites for lithium migration and are therefore less impacted by the presence of the immobile alkali earth ions. Further studies of *A*-site aliovalent substitution in A_3MX_6 materials are necessary to understand the interplay of mobile ion vacancies and the dimensionality of the migration pathways.

X-*site aliovalent substitution.*—Aliovalent substitution at the halide *X* site is the least commonly observed modification in the A_3MX_6 family. Unlike substitution at the *A* or *M* sites, it is not possible to form donor defects that modulate the concentration of alkali ion vacancies through aliovalent substitution at the *X* site. Sulfide (S^{2-}) is the most probable aliovalent substitution at the halide site, as sulfide has a similar ionic radius to chloride and sulfide/halide mixing is well-known in other solid electrolyte families (*e.g.*, Li_6PS_5Cl,[63] $Li_{4.3}AlS_{3.3}Cl_{0.7}$[64]). In the A_3MX_6 family,

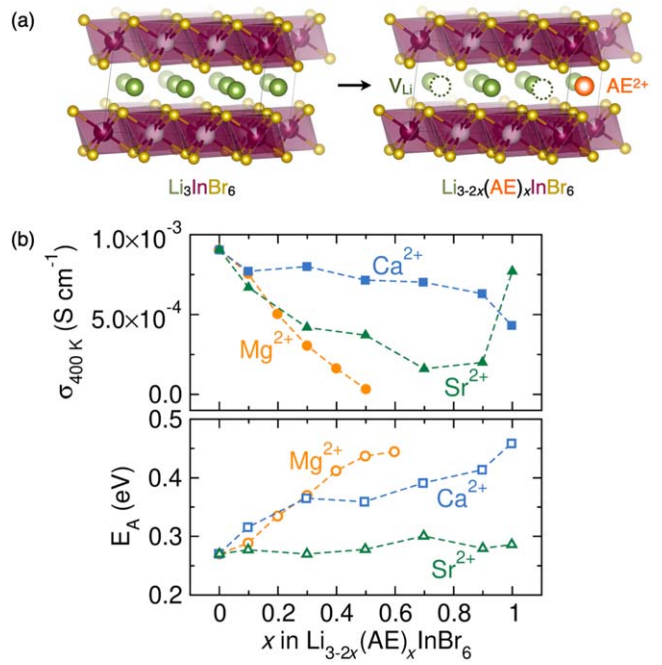

Figure 7. Aliovalent substitution of varying alkali earth (*AE*) ions at the *A* site raises decreases Li-ion conductivity and raises the activation barrier in the superionic phase of Li_3InBr_6. A structural schematic illustrating how divalent AE^{2+} ions are compensated by Li^+ vacancies in $Li_{3-2x}(AE)_xInBr_6$ is shown in (a). Experimental ionic conductivities and activation barriers measured for varying *AE* ions is shown in (b). Data in (b) are reproduced from Tomita et al.[60]

the excess negative charge of the sulfide ion may be compensated by a halide vacancy, by the inclusion of excess alkali ion ($Li_{3+x}MCl_{6-x}S_x$), or by the inclusion of excess trivalent metal ions ($Li_3M_{1+\frac{1}{3}x}Cl_{6-x}S_x$). Electronic charge compensation by excess holes will likely incur a large energy penalty to further oxidation due to the filled octets of the constituent ions. To our knowledge, there has only been one report of aliovalent sulfide substitution in Li_3InCl_6 by Yamagishi et al.,[65] though the compensation mechanism and electrochemical properties of the substituted material have not yet been reported.

While aliovalent halide substitution by sulfide will not likely provide desirable defect compensation mechanisms for vacancy tuning, the large polarizable sulfide ion can potentially impact ion transport properties through other mechanisms. The larger size of S^{2-} compared to Cl^- expands the unit cell volume in $Li_3In(Cl:S)_6$,[65] which may yield larger bottleneck sizes for ion diffusion and reduced activation barriers. Halide/sulfide site disorder is also well-known to reduce activation barriers across a variety of solid electrolyte chemistries (*i.e.*, Li_6PS_5Br,[66] $Li_{4.3}AlS_{3.3}Cl_{0.7}$,[64] $Li_{6-x-2y}Ca_yPS_{5-x}Cl_{1+x}$[62]) and such disorder may provide a similar effect in substituted alkali metal halides. Finally, the soft and polarizable sulfide ion may soften the potential energy landscape experienced by the mobile ions to reduce activation barriers for ion conduction.[67,68] Altogether, these effects have been demonstrated to lower the activation barriers for ion conduction in other materials families, but are still unexplored in the A_3MX_6 family.

Isovalent Substitution

While aliovalent substitution provides more possibilities for increasing ionic conductivity through systematic increases in defect concentrations and lowering of ion migration barriers, isovalent substitution can similarly influence the host lattice structure to enhance ion conduction. Isovalent substitution or alloying occurs when ions in the host structure are replaced by differing guest ions with the same formal charge. As the substituted ion does not directly induce a change in the concentration of defects by changing ionic charge, the primary impacts to the ionic conductivity are the result of manipulations to the host structure to influence the migration barrier (E_m). Substituting ions of differing size and polarizability induces changes in the volume of ion migration pathways and influences local bonding environments, ion migration energy barriers, and lattice dynamics to impact ion transport.

M-*site isovalent substitution.*—*M***-site isovalent substitutions involve partially replacing with another cation in 3+ formal oxidation state. As discussed previously, the *M*-site cation greatly influences the structure of the A_3MX_6 solid electrolyte. As such, *M*-site isovalent substitutions may be categorized into alloys that are: (1) isostructural, and (2) heterostructural. When *M*-site substitution does not trigger a global structural change, it is considered an isostructural alloy and changes in Li-ion conductivity and other properties are attributed to local effects. Heterostructural alloying, on the other hand, is accompanied by structural changes as a function of degree of substitution. Here, both global and local effects contribute to battery-relevant properties, including Li-ion conductivity and electrochemical stability.

Studies that have investigated the effect of *M*-site isovalent substitutions (or alloying) are limited to heterostructural In^{3+} substitution in $Li_3Y_{1-x}In_xCl_6$. Li et al. found that increasing In content triggers a structural change from the metastable orthorhombic Li_3YbCl_6-type (*Pnma*) at $x = 0$ to trigonal Li_3YCl_6-type ($P\bar{3}m1$) at $x = 0.1$ to monoclinic 2D Li_3ScCl_6 ($C2/m$) for $x > 0.2$.[6] The transition from hcp structures to the ccp Li_3ScCl_6 structure is accompanied by a 10-fold enhancement in the room-temperature Li-ion conductivity for $x = 0.2$, as shown in Fig. 8. The substantial increase in ionic conductivity is attributed to the ccp sublattice, likely due to the lower packing density compared to hcp structures.[69] Given the diversity of structures in the A_3MX_6 family of solid electrolytes and the ability to control halide close-packing by tuning the composition, it will be worthwhile to explore the rich and vast phase space of heterostructural alloys realized through isovalent substitutions.

In the absence of bulk structural changes, *M*-site isovalent substitution can also impact ion transport by tuning the volume of the migration pathways. Wan and Ciucci computationally investigated the effect of Sc^{3+} and La^{3+} isovalent substitutions on ion transport in Li_3YCl_6.[58] The authors found that substitution of Sc^{3+} is energetically favorable compared to La^{3+}, which correlates with their ionic radii relative to Y (smaller Sc^{3+} $r = 0.75$ Å, larger La^{3+} $r = 1.03$ Å). From *ab initio* molecular dynamics simulations, expansion of the ion migration pathways with substitution of the larger La^{3+} is predicted to lower the activation barrier and improve Li-ion conductivity relative to the unsubstituted Li_3YCl_6.

Liu et al.[70] systematically explored the Li chlorides in the Inorganic Crystal Structure Database (ICSD) with fcc and hcp anion sublattices and identified 20 unique structures with renormalized compositions that can be represented by Li_xMCl_4, by $Li_xM_{2/3}Cl_4$, and by $Li_xM_{1/2}Cl_4$. Using high-throughput density functional theory (DFT) calculations, isovalent and aliovalent substitutions were performed to realize hypothetical structures that were assessed for their phase stability, electrochemical stability window, and Li ion conductivity. In addition to aliovalent substitutions, the study provides insights into the effect of isovalent substitutions on the Li substructure. The existence of Li_xAlCl_4 phases also suggest the possibility of Al isovalent substitutions in Li_3MX_6, even though Li_3AlX_6 does not exist or has not been experimentally realized.

A-*site isovalent substitution.*—*A***-site isovalent substitution in the A_3MX_6 family and the influence on ion transport are not yet reported, but we can develop predictions for the resultant properties based on the effects of alkali substitution in other solid electrolyte systems. The "mixed alkali effect" has a pronounced and detrimental effect on the ionic conductivity in the β-alumina-type solid electrolytes. Gradual sodium substitution for potassium in K-β-gallate is

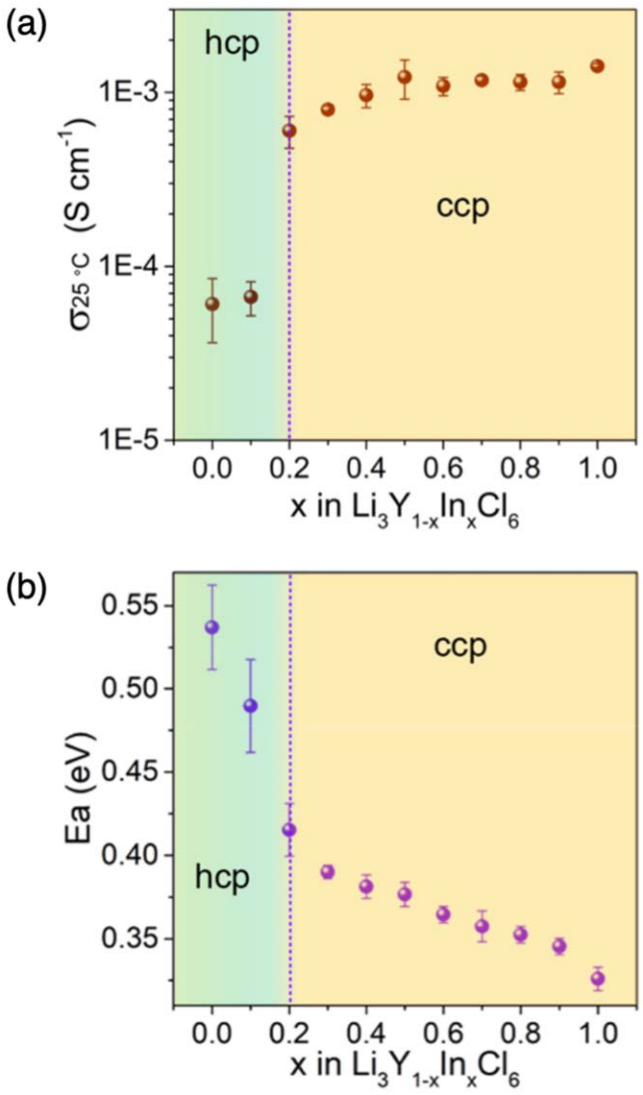

Figure 8. Impact of isovalent *M*-site substitution on (a) room temperature ionic conductivity and (b) activation barrier in $Li_3Y_{1-x}In_xCl_6$. The vertical line and shaded regions at 20% In substitution denote the transition between the hcp and ccp structures. Portions of this Fig. are reproduced with permission from Ref. 6 ©2020 American Chemical Society.

accompanied by a sharp, non-linear decrease in ionic conductivity at 20% Na^+.[71] A similar effect is found when Na^+ is gradually replaced with Li^+ ions in β-alumina.[72] This effect has been explained in the context of percolation theory, where local ordering of the alkali ions at the percolation threshold creates a stabilizing effect that raises the activation barriers for ion conduction.[73]

Beyond the "mixed alkali effect", alkali substitution can impact the observed structure type, and therefore the ion migration pathways, of the A_3MX_6 family. As illuminated in Table I, many of the Na-based metal halides adopt the cryolite "double perovskite" structure type, while other structure types are observed for the Li-based analogs. Similarly, perovskite-like structural topologies are also observed for the larger alkali ions. One consequence of alkali substitution is the potential formation of cation-ordered perovskite phases when $^2/_3$ of the Li^+ or Na^+ ions are replaced with larger alkalis. For example, replacing two Li^+ ions with Cs^+ to form Cs_2LiMX_6 results in an ordered double perovskite ("elpasolite") structure type, in which the Li^+ and Cs^+ cations form an ordered sublattice.[74] To our knowledge, the elpasolite family does not exhibit appreciable ionic conductivity.

Between the "mixed alkali effect" and the formation of non-conducting structure types, we anticipate that alkali mixing will be detrimental to ion transport properties in the A_3MX_6 family.

X-*site isovalent substitution.*—Halide substitution directly impacts the physical volume of the ion migration pathways in the A_3MX_6 family of materials. Early studies by Tomita et al. demonstrated the impact of halide substitutions on the structure and ionic conductivity of Li_3InBr_6.[75] Substitution of Br^- with I^- was found to expand the volume of the unit cell and yielded the highest ionic conductivity and lowest activation barrier for $Li_3InBr_3I_3$. In contrast, F^- substitution resulted in a contraction of the lattice and a reduction in the ionic conductivity.[75] The differences in ion transport between the F^-- and I^--substituted analogs are attributed to changes in the volume of the migration pathways and the polarizability of the halide (to be discussed in greater detail below). In contrast, chloride substitution has a unique impact on the structure and ionic conductivity in $Li_3InBr_{6-x}Cl_x$. Li_3InBr_6 is reported to undergo a phase transition above $T = 314$ K to a superionic phase that is isomorphous with Li_3InCl_6.[76] Interestingly, chloride substitution stabilizes the superionic phase below room temperature for $x \geqslant 3$ in $Li_3InBr_{6-x}Cl_x$ and subsequently yields higher room-temperature ionic conductivities for the substituted analogs despite the decrease in lattice volume.[17] The highest ionic conductivity found for $Li_3InBr_3Cl_3$ has been explained by considering changes in the character of the $LiCl_6$ vs $LiBr_6$ bonding environments.[77]

In addition to the physical size of the migration pathways, the halide sublattice also dictates the observed structure type and anion close-packing. For example, Li_3YCl_6 adopts the 1D trigonal structure type ($P\bar{3}m1$) with an hcp sublattice, while Li_3YBr_6 adopts the layered Li_3ScCl_6 structure type ($C2/m$) with a ccp sublattice.[46] When alloyed, $Li_3YCl_3Br_3$ appears to adopt the ccp monoclinic structure familiar to the bromide and is reported to achieve room-temperature ionic conductivities up to 7.2×10^{-3} S cm^{-1}. This increase in conductivity can be attributed to occupancy of Li ions in the tetrahedral interstitial sites enabled by the halide alloying coupled with the lower-density ccp structure that facilitates higher ionic conductivities.[18]

Halide substitution further offers a handle to tune the polarizability and mechanical properties of metal halide solid electrolytes to impact a suite of battery-relevant properties. Generally, solid electrolytes with softer and more polarizable frameworks tend to exhibit lower activation barriers and higher ionic conductivities, as more polarizable anion species screen the charge of the mobile ions to weaken the interactions between the mobile ion and the host framework. Mechanically softer structures also exhibit lower-energy lattice vibrations that can assist in ion migration to lower the activation barriers.[68,78,79] Mechanically-soft solid electrolytes also hold promise for use with lithium metal anodes, as they are hypothesized to prevent the growth of parasitic Li dendrites that result in premature battery failures.[80] Calculations of the elastic properties of the Li_3MX_6 solid electrolytes illustrate that larger halides universally produce mechanically softer materials regardless of the choice of *M*-site cation.[24] The trends in mechanical properties are also generally correlated with ion transport properties. As discussed above, I^- substitution in Li_3InBr_6 increases the ion diffusivity while the opposite trend is observed for F^- substitution.[75] This behavior is supported by a computational study of the Li_3YX_6 series by Wan et al., which demonstrated that the higher Bader charge on both F^- and Li^+ and shorter Li–F distances resulted in higher ionicity of the Li–F interactions that stabilized the Li ions at the octahedral sites compared to the other members of the halide series.[58]

It is important to note that the impacts of halide substitution (*e.g.*, bottleneck size, structure type, mechanical properties) on ion transport occur in tandem and their contributions cannot be easily isolated. This is exemplified by $Li_3InBr_{6-x}Cl_x$ and $Li_3YCl_{6-x}Br_x$; the highest ionic conductivities were found at the 50% alloy

compositions due to a "Goldilocks" combination of lattice volume, polarizability of the Li–*X* bonding environment, and stabilization of structure types that enable high ionic conductivity.[24,58,75]

Electrochemical Stability

Understanding the impact of chemical modifications on the electrochemical stability of SEs is paramount to their performance in full-cell battery architectures. In the present context, we refer to the electrochemical stability window as the voltage range over which the electrolyte does not participate in charge-transfer reactions with the electrodes. The electrochemical stability window is dictated by several metrics, including alignment of the valence and conduction band edges of the electrolyte with respect to the Fermi level of the electrodes, the stability of the electrolyte with respect to changes in mobile ion concentration, and the phase stability of the electrolyte with respect to the chemical potential of the constituent elements.[81,82] Here, we discuss how substitutions in the A_3MX_6 family impact their electrochemical stability windows in the context of the conduction and valence band alignments and in the context of phase stability.

Band-edge approach to electrochemical stability.—Within the band-edge approach to electrochemical stability, the electrolyte is considered stable against oxidation if the energy of the valence band maximum relative to vacuum (the ionization potential) is lower in energy than the Fermi level of the cathode. Conversely, the electrolyte is considered stable to reduction if the energy of the conduction band minimum relative to vacuum (the electron affinity) resides above the Fermi level of the anode.[24,46] Wider band gaps are therefore typically correlated with improved electrochemical stability of SEs.

We have constructed molecular orbital theory diagrams of a single MX_6 octahedron to provide qualitative insights into the impact of both isovalent and aliovalent substitutions on the electrochemical stability windows in this material family. We first consider the symmetry-adapted linear combinations (SALCs) of the halide ligand group orbitals in combination with the frontier atomic orbitals of the trivalent metal. Each of the six halides contributes three filled *p* orbitals. Within the O_h point group of the octahedron, this produces 6 σ-bonding ($\Gamma_{red} = A_{1g} + E_g + T_{1g}$) and 12 π-bonding ($\Gamma_{red} = T_{1g} + T_{2g} + T_{1u} + T_{2u}$) SALCs (Fig. 9). The six halides bring 36 total electrons and each ligand group orbital is fully occupied. When the metal site is occupied by a Group 13 *p*-block metal (*i.e.*, In^{3+}, Ga^{3+}, Al^{3+}), the A_{1g} and T_{1u} group orbitals have the appropriate symmetry and energy to interact with the empty *s* and *p* orbitals of the metal, producing a σ/σ^* set with A_{1g} symmetry and one σ/σ^* and two π/π^* sets with T_{1u} symmetry. The remaining SALCs (T_{1g}, T_{2u}, E_g, T_{2g}) form a manifold of occupied non-bonding halide states that do not possess the correct symmetry to undergo bonding interactions and thus comprise the highest occupied states. The lowest unoccupied states are dictated by the antibonding A_{1g}^* states derived from hybridized $M\,s - X\,p$ states. When the metal site is occupied by a transition metal (*i.e.*, Sc^{3+}, Y^{3+}, Zr^{4+}, Hf^{4+}), the *d* orbitals of the metal are permitted to engage in bonding with the formerly non-bonding E_g and T_{2g} ligand group orbitals, as shown in Fig. 9. If the transition metal *d* orbitals are empty (d^0), then the remaining non-bonding halide SALCs (T_{1g}, T_{2u}) comprise the highest occupied states, while the T_{2g}^* π^* set dictates the lowest unoccupied states.

From this simplified molecular orbital theory approach, we can construct a set of guiding principles for how composition and substitutions impact the upper bounds on the electrochemical stability windows in the A_3MX_6 family. We find that the ionization potential is pinned at the halide non-bonding states and the oxidative stability is therefore dictated by the choice of the halide. This observation is consistent with the observed trends in oxidative stability across the halide series ($F^- > Cl^- > Br^- > I^-$) shown in Fig. 10a.[24,46,58] This conclusion also holds implications for the incorporation of aliovalent anions at the halide site. For example, incorporating the less electronegative S^{2-} ion will likely push the ionization potential to higher energies and reduce stability at higher voltages. From this analysis, we can conclude that metal-site substitutions will not likely impact the oxidative stability to a first approximation, assuming that the metal is not redox active. This is illustrated by the example of $Li_{2.9}In_{0.9}Zr_{0.1}Cl_6$, which demonstrated comparable oxidative stability to the parent Li_3InCl_6 (Fig. 10b).[12]

The interaction between the *M* and *X* electronic states dictates the reductive stability of the A_3MX_6 SEs. This is exemplified by the differences in the reductive stability for different *M*-site ions (Fig. 10a). When the *M* site is occupied by a *p*-block metal (*e.g.*, In^{3+}, Bi^{3+}), the lowest unoccupied state is derived from the A_{1g}^* state, which resides at lower energies compared to the T_{2g}^* set that forms when the *M* site is occupied by a *d*-block metal (Fig. 9) and produces a smaller bandgap. The smaller bandgap and lower lying states result in a higher reduction potential of ~2.4 V for In^{3+} and Bi^{3+} compared to <1 V (vs Li/Li^+) for the *d*- and *f*-block analogs.[24]

Using this MO theory approach, we can predict the impact of substitutions on the electrochemical stability window. As shown in Fig. 9, Zr^{4+} substitution for In^{3+} results in the formation of the antibonding T_{2g} π^* set at higher energies than the A_{1g}^* set and will likely improve the reductive stability. This notion is consistent with a computational study by Kim et al.[24] As the electron affinity is dictated by the $M - X$ interaction, halide substitution also plays a role in determining reductive stability. For example, fluoride substitution in $Li_3YBr_{5.7}F_{0.3}$ improves the reductive stability relative to Li_3YBr_6 and enables stable cycling against lithium metal (Fig. 10c).[83]

The impact of isovalent subtitution at the *M* site on electrochemical stability windows has been explored computationally in study by Wan and Ciucci.[58] As expected from the MO theory diagram, substitution of Sc^{3+} and La^{3+} in Li_3YCl_6 does not impact the oxidative stability that is dictated solely by the chloride states. The reductive stability limits proceed as $Li_3Y_{5/6}La_{1/6}Cl_6 \approx Li_3YCl_6 < Li_3Y_{5/6}Sc_{1/6}Cl_6$. The higher reductive stability of the Sc^{3+}-substituted material is attributed to the higher electronegativity of Sc^{3+} compared to Y^{3+}, which likely pushes the lowest unoccupied states to higher energy.

Furthermore, this analysis also demonstrates that, in order to retain the desirable electrochemical stability of the host material, substituting ions should possess a filled shell such that they do not contribute excess electrons that will populate the anti-bonding states at the conduction band minimum. This can be rationalized by considering the MO diagram for the transition metal chloride octahedron in Fig. 9. The lowest unoccupied states are derived from the empty T_{2g}^* states. However, the inclusion of excess *d* electrons would occupy the T_{2g}^* set and would substantially impact the oxidative stability limits of the electrolyte. We emphasize that this MO theory approach does not account for phase stability of the electrolyte nor the chemical reactions that may occur at the electrode-electrolyte interfaces. Rather, this method provides a simple and approximate prediction for how substitutions can impact the electrochemical stability.

Phase stability.—Although we have demonstrated that a simplified MO theory approach can predict how substitutions will affect the upper limits of the electrochemical stability window, the phase stability of the SE in contact with electrodes or with respect to the chemical potentials of the constituent elements is critical for practical device performance. Unfortunately, identifying the chemical stability of an electrolyte and the potential decomposition pathways are not as easily predicted without enlisting first-principles quantum mechanical calculations to obtain total energies.

We first consider the phase stability of the A_3MX_6 family and potential decomposition reactions with electrode chemistries. Kim

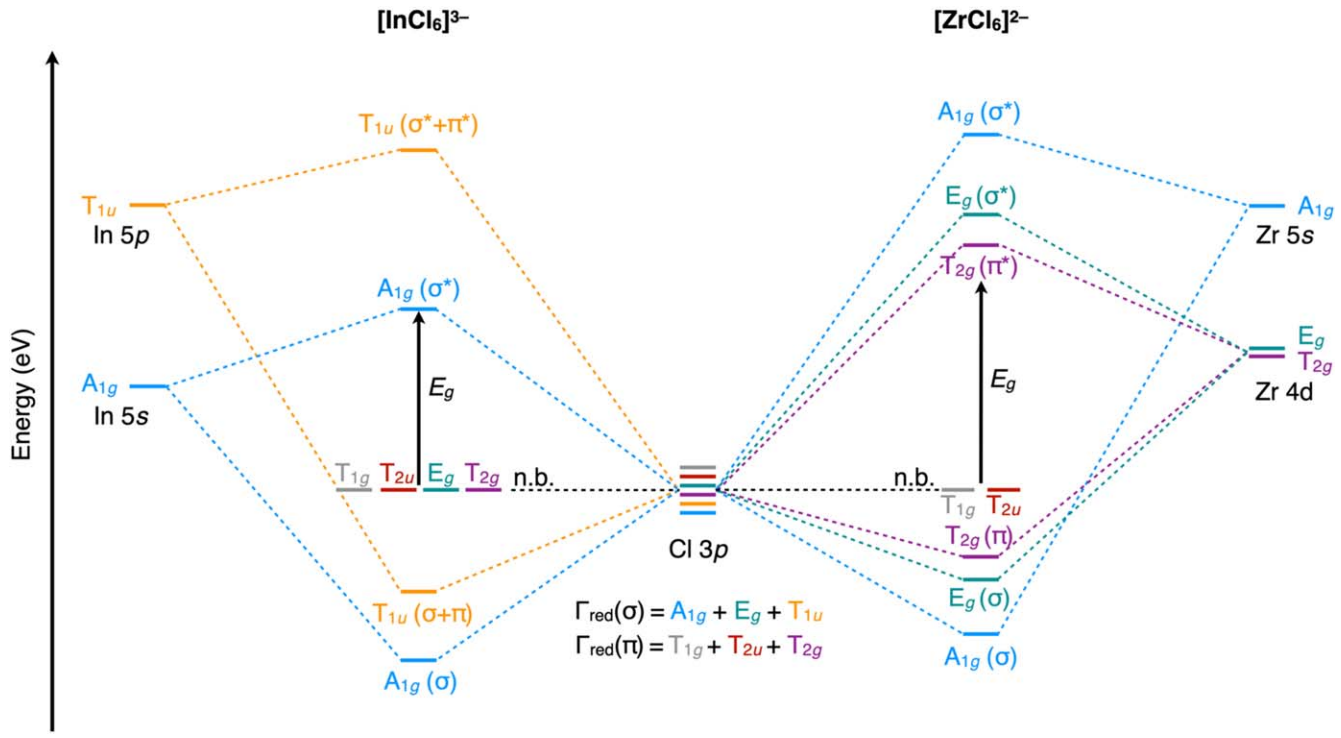

Figure 9. Molecular orbital theory diagram of an $[InCl_6]^{3-}$ octahedron and a $[ZrCl_6]^{2-}$ octahedron demonstrating how Zr^{4+} substitution in $Li_{3-x}In_{1-x}Zr_xCl_6$ impacts the character of the frontier states. The highest occupied states are derived from the non-bonding (n.b.) halide states, while the lowest unoccupied states are derived from the antibonding metal-halide states. The energy gap (E_g) is highlighted by the arrow between these states.

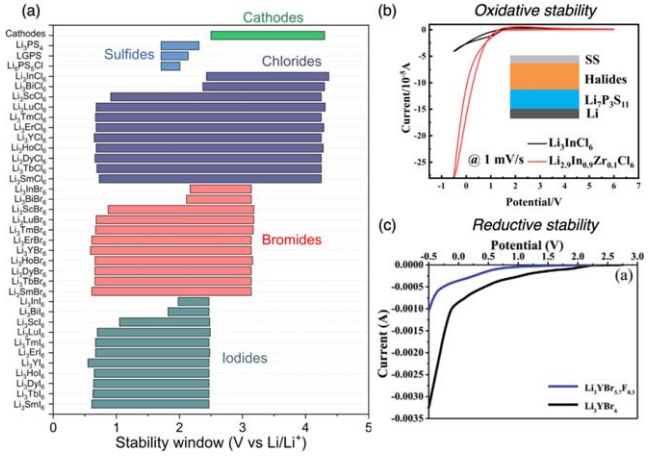

Figure 10. (a) Electrochemical stability windows of varied solid electrolytes of the A_3MX_6 family (Fig. reproduced with permission from 24 ©American Chemical Society). In (b), Zr^{4+} substitution in Li_3InCl_6 does not impact oxidative stability relative to the unsubstituted parent compound (Fig. reproduced with permission from 12 ©2021 American Chemical Society). In (c), fluoride substitution in $Li_3YBr_{5.7}F_{0.3}$ improves reductive stability (Fig. reproduced with permission 83 ©2021 John Wiley and Sons).

et al. used computations to identify the decomposition products of the Li_3MX_6 family with oxide cathodes and lithium metal. Across various oxide cathodes, including $LiMn_2O_4$ (LMO), $Li(NiMnCo)_{1/3}O_2$ (NMC), and $LiCoO_2$ (LCO), common decomposition products of the Li_3MX_6 family include the binary phases LiX and M_2O_3.[24] When in contact with lithium metal, the decomposition is driven by the reduction of the trivalent metal species to elemental M^0 for *d*- and *f* -block analogs or by the formation of $Li-M$ alloys for Li_3InX_6 and Li_3BiX_6.[24]

As the decomposition and phase stability are dictated by the *M*- and *X*-site ions, both aliovalent and isovalent substitutions at these sites are expected to alter phase stability and decomposition pathways. Kim et al. used first-principles calculations to evaluate how Zr^{4+} substitution impacts the phase stability of Li_3InCl_6 and Li_3YCl_6.[24] Zr^{4+} substitution in Li_3InCl_6 does not appear to substantially impact the electrochemical stability compared to the parent compound. As supported by our MO theory diagram (Fig. 9), the Zr–Cl anti-bonding states reside at higher energies than the In–Cl states and therefore do not significantly impact the reductive stability. Reaction of $Li_{2.5}In_{0.5}Zr_{0.5}Cl_6$ with oxide cathodes is predicted to form ZrO_2 as a decomposition product, which likely reduces the oxidative stability relative to the parent compound.[24] In contrast, Zr^{4+} substitution in Li_3YCl_6 substantially impacts the electrochemical stability compared to the parent compound. Zr^{4+} substitution substantially lowers the bandgap relative to the parent compound, likely due to mixing of Zr–Cl vs Y–Cl hybridized states at the conduction band minimum. At oxidizing potentials, the inclusion of Zr^{4+} favors the formation of ZrO_2 phases and results in poorer oxidative stability. At reducing potentials, the formation of zirconium chlorides raises the reduction potential by nearly 1 V.[24]

We hypothesize that the distinct differences in phase stability for Zr^{4+} substitution in Li_3InCl_6 vs Li_3YCl_6 may arise from structural differences that dictate the solubility limits of Zr^{4+} into the respective structures. Li_3InCl_6 and Li_2ZrCl_6 adopt nearly identical monoclinic structures (2D Li_3ScCl_6 structure type) that enables alloying between the two compositions.[15] In contrast, Li_3YCl_6 adopts the trigonal $P\bar{3}m1$ structure type and experimental studies demonstrate that only 20% Zr^{4+} is permitted to substitute before different structure types are observed.[54] We suspect that these structural differences impact the proclivity of a given substituted material to undergo decomposition reactions with the electrodes.

Electronic conductivity.—Lastly, we address the subject of electronic conductivity in aliovalently-doped A_3MX_6 SEs, which currently does not garner enough discussion. Most SEs, including oxides, sulfides, and halides typically have ultra-wide band gaps (>4 eV) and therefore, the argument that large bandgap materials

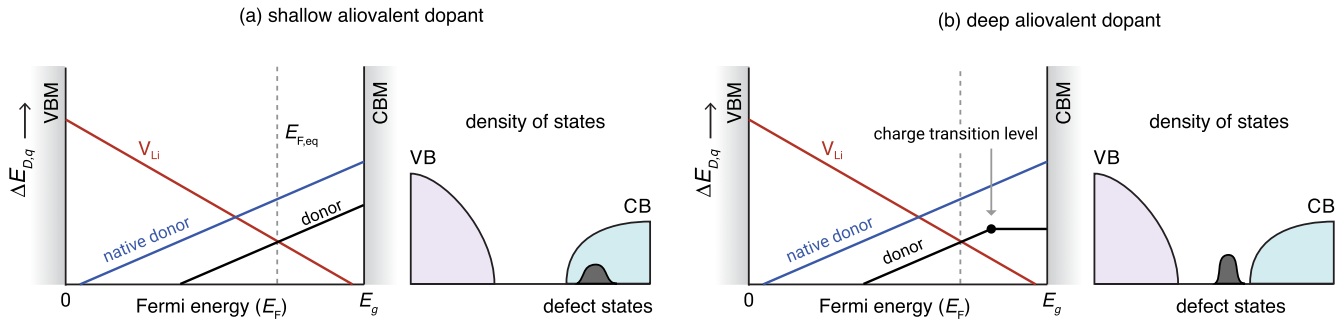

Figure 11. Shallow vs. deep nature of defects dictate whether the associated electronic charge is delocalized or bound to the defects. (a) Defect diagram and electronic density of states of a typical shallow donor defect, characterized by the absence of charge transition levels (CTLs) in the defect diagram and presence of resonant states inside the conduction band. (b) Deep defects are characterized by CTLs (location of defect states) away from the corresponding band edges by more than a few k_BT. Presence of mid gap states is a feature of such deep defects; the associated charge is localized or bound to the defect, unlike in shallow defects where they are delocalized.

tend to be electronic insulators is often invoked to suggest low electronic conductivities. Fundamentally, it is the concentration and nature (deep vs. shallow) of the charged defects in a SE that determine the free electronic conductivity. The tendency of large bandgap materials to be electronic insulators is an empirical observation, but not rooted in the fundamental origin of electronic conductivity.

Recent studies have highlighted the issues of electronic conductivity (σ_e) in SEs. Han et al. demonstrated that σ_e as low as 10^{-9} S cm^{-1} can trigger nucleation and growth of Li dendrites in SEs.[84] It suggests that the ratio of electronic to ionic conductivity may not be a sufficient criterion to gauge whether the SE is prone to Li dendrite formation. Gorai et al. have shown through detailed first-principles defect calculations that the experimentally-observed σ_e in topical Li- and Na-ion SEs are due to the presence of charged point defects in the bulk, even in undoped SEs.[85] In doped SEs, the condition is further exacerbated because of the creation of additional electronic carriers (electrons, holes).

While measurements of electronic conductivity in doped A_3MX_6 SEs are often not available, first-principles defect calculations may provide insights into the concentration of electronic carriers and whether they are free carriers that contribute to electronic conductivity or bound to defects as localized carriers. Figure 11 illustrates two scenarios for an aliovalent donor dopant: (a) shallow donor, and (b) deep donor. In a defect diagram, this is gleaned from the charge transition levels (CTLs), which are the Fermi energy E_F at which the favorable charge state of the defect changes, as identified by kinks in the defect lines (Fig. 11b). CTLs correspond to the location of defect states in the bandgap.

Shallow donors introduce defect states that are either resonant with the conduction band or introduce defect states close to the conduction band edge, typically within a few k_BT (k_B is Boltzmann constant). Ionized shallow donors will contribute free electrons to the conduction band, and therefore, directly increase σ_e. Therefore, shallow defects are identified by either an absence of CTLs within the bandgap or CTLs close to the corresponding band edge, as shown in the case of a shallow donor dopant in Fig. 11a. In contrast, deep defects introduce states within the bandgap and are responsible for trapping electronic carriers (Fig. 11b). In other words, electronic carriers are bound to deep defect states and cannot be ionized to form free electrons or holes. In principle, bound (or localized) carriers cannot contribute to σ_e and therefore are desired to minimize σ_e. In addition, the presence of impurity phases or extended defects, such as grain boundaries and decomposition phases at the interfaces with the electrodes, may also affect σ_e in real samples.

As A_3MX_6 SEs garner more interest, there will be increased efforts to improve ionic conductivity through aliovalent and isovalent substitutions beyond the handful that have been discussed in this Review. In this context, we propose the following doping design considerations with a focus on electronic conductivity: (1) substitutions should not increase σ_e beyond 10^{-9}–10^{-10} S cm^{-1}, (2) aliovalent dopants that increase ionic conductivity and introduce deep defect states are desirable (vs. shallow states), and (3) σ_e should be rigorously and systematically measured in doped A_3MX_6 SEs.

Outlook and Future Directions

Chemical modifications of A_3MX_6 solid electrolytes through substitution at the *A*, *M*, and *X* sites have proven to be an effective strategy to achieving high ionic conductivities, good electrochemical compatibility with common electrode chemistries, and improved environmental stability. Yet the relative nascence of these materials as SEs and the modest number of studies focused on substitutions presents several opportunities for future study, which we enumerate below.

- Aliovalent substitutions have thus far been focused almost exclusively on Zr^{4+} substitution on the trivalent *M*-site cation. Identifying other substituting ions for all three sites in A_3MX_6 would expand the suite of chemical substitutions and deliver a more complete understanding of the roles of substituting ion size, polarizability, and structure preference in ion transport in this family of materials. Along with further studies of aliovalent Zr^{4+} and Hf^{4+} substitution, potential candidates to explore for other metal ion substitutions are higher-valency metals such as niobium (Nb^{5+}) or tantalum (Ta^{5+}); the increased stability of the higher oxidation states of both ions lends them to better reductive stability compared to first-row transition metals.[86] Additionally, the higher charge difference between Nb^{5+}/Ta^{5+} and the host M^{3+} may offer an opportunity to introduce a larger number of mobile ion vacancies for smaller concentrations of substituting ions. Even though the ionic radii of Nb^{5+}/Ta^{5+} ($r = 64$ pm)[53] would contract the unit cell volume, the lower degree of substitution required to generate the same number of mobile ion vacancies could decouple the impacts of vacancies and lattice volume on ionic conductivity. Molybdenum and tungsten may also provide a similar avenue for aliovalent substitution, although the greater number of stable oxidation states for these ions would be detrimental to the electrochemical stability.
- Given the broad range of chemistries and substitutions that are accessible at all three sites in the A_3MX_6 family, it is necessary to develop methods to *a priori* identify which substituting ions and concentrations provide desirable properties. Presently, substitutions in the ternary metal halides are explored through time-consuming systematic experimental studies using chemical intuition to identify substituting ions. Defect diagrams have historically been calculated to identify defects and compensation mechanisms for doping in semiconductors, and have recently been applied to substitutions in solid electrolytes.[85,87–90] In future studies, leveraging these computational methods could guide experimental studies and enable rational design of substituted ternary metal halides.

- While some members of the A_3MX_6 family are reported to be relatively tolerant to ambient humidity,[6] the impact of substituting ions on the environmental stability of these materials has not yet been explored in depth. In metal halide perovskites, substitutions at both the cation and anion sites have been demonstrated as an effective strategy for improving moisture tolerance,[91] an approach that may be further extended to substitutions in metal halide solid electrolytes. In theory, first-principles DFT calculations can be used to assess the phase stability of substituted Li_3MX_6 against decomposition into competing hydrated binary and other phases. Further efforts in this area are needed to understand how these substitutions impact air- and moisture-tolerance of these materials.
- Finally, this Review has focused exclusively on substitutions in the A_3MX_6 family of solid electrolytes, yet several families of ternary metal halides of differing stoichiometries (*i.e.*, AMX_4, A_2MX_4) have been identified as potential materials for energy storage applications.[19,70] So far, the impact of chemical substitutions in these materials is relatively unexplored. Future avenues of research may focus upon expanding the design principles for substitution in the A_3MX_6 family to other ternary metal halides.

Conclusions

Ternary metal halides of the general formula A_3MX_6 are an exciting family of solid electrolytes for all-solid-state batteries that occupy a rich structural and compositional phase space. In this Review, we have identified the materials design principles that govern how chemical substitutions at all three sites can impact properties that are relevant for applications in all-solid-state batteries. Further, we have identified future avenues of research in this exciting family of materials. Understanding how changes in composition and structure can elicit desirable functional properties will enable transformative advances for all-solid-state batteries and beyond.

Acknowledgments

The authors thank Prof. Saneyuki Ohno (Kyushu University) for useful discussions. This work was conducted by the Alliance for Sustainable Energy, LLC, the manager and operator of the National Renewable Energy Laboratory for the U.S. Department of Energy (DOE) under Contract No. DE-AC36-08GO28308. This research was supported by the Laboratory Directed Research and Development (LDRD) program at NREL. The views expressed in the article do not necessarily represent the views of the DOE or the U.S. Government.

ORCID

Sinclair R. Combs https://orcid.org/0000-0002-8982-0288
Paul K. Todd https://orcid.org/0000-0001-5409-3634
Prashun Gorai https://orcid.org/0000-0001-7866-0672
Annalise E. Maughan https://orcid.org/0000-0002-3292-4799

References

1. J. B. Goodenough and Y. Kim, "Challenges for rechargeable Li batteries." *Chem. Mater.*, **22**, 587 (2009).
2. J. Janek and W. G. Zeier, "A solid future for battery development." *Nat. Energy*, **1**, 1 (2016).
3. T. Asano, A. Sakai, S. Ouchi, M. Sakaida, A. Miyazaki, and S. Hasegawa, "Solid Halide Electrolytes with High Lithium-Ion Conductivity for Application in 4 V Class Bulk-Type All-Solid-State Batteries." *Adv. Mater.*, **30**, 1 (2018).
4. G. Xu et al., "Origin of High Electrochemical Stability of Multi-Metal Chloride Solid Electrolytes for High Energy All-Solid-State Lithium-Ion Batteries." *Nano Energy*, **92**, 106674 (2022).
5. X. Li et al., "Water-Mediated Synthesis of a Superionic Halide Solid Electrolyte." *Angew. Chem.*, **131**, 16579 (2019).
6. X. Li et al., "Origin of Superionic $Li_3Y_{1-x}In_xCl_6$ Halide Solid Electrolytes with High Humidity Tolerance." *Nano Lett.*, **20**, 4384 (2020).
7. W. Li et al., "Unraveling the origin of moisture stability of halide solid-state electrolytes by in situ and operando synchrotron X-ray analytical techniques." *Chem. Mater.*, **32**, 7019 (2020).
8. C. Wang et al., "Interface-assisted in-situ growth of halide electrolytes eliminating interfacial challenges of all-inorganic solid-state batteries." *Nano Energy*, **76**, 105015 (2020).
9. C. Wang et al., "A universal wet-chemistry synthesis of solid-state halide electrolytes for all-solid-state lithium-metal batteries." *Sci. Adv.*, **7**, 1 (2021).
10. R. Schlem, A. Banik, M. Eckardt, M. Zobel, and W. G. Zeier, "$Na_{3-x}Er_{1-x}Zr_xCl_6$-A halide-based fast sodium-ion conductor with vacancy-driven ionic transport." *ACS Appl. Energy Mater.*, **3**, 10164 (2020).
11. E. A. Wu et al., "A stable cathode-solid electrolyte composite for high-voltage, long-cycle-life solid-state sodium-ion batteries." *Nat. Commun.*, **12**, 1 (2021).
12. X. Luo, X. Wu, J. Xiang, D. Cai, M. Li, X. Wang, X. Xia, C. Gu, and J. Tu, "Heterovalent Cation Substitution to Enhance the Ionic Conductivity of Halide Electrolytes." *ACS Appl. Mater. Interfaces*, **13**, 47610 (2021).
13. S. Y. Kim, K. Kaup, K. H. Park, A. Assoud, L. Zhou, J. Liu, X. Wu, and L. F. Nazar, "Lithium Ytterbium-Based Halide Solid Electrolytes for High Voltage All-Solid-State Batteries." *ACS Mater. Lett.*, **3**, 930 (2021).
14. J. Park, D. Han, H. Kwak, Y. Han, Y. J. Choi, K. W. Nam, and Y. S. Jung, "Heat treatment protocol for modulating ionic conductivity via structural evolution of $Li_{3-x}Yb_{1-x}M_xCl_6$ ($M = Hf^{4+}$, Zr^{4+}) new halide superionic conductors for all-solid-state batteries." *Chem. Eng. J.*, **425**, 130630 (2021).
15. B. Helm, R. Schlem, B. Wankmiller, A. Banik, A. Gautam, J. Ruhl, C. Li, M. R. Hansen, and W. G. Zeier, "Exploring Aliovalent Substitutions in the Lithium Halide Superionic Conductor $Li_{3-x}In_{1-x}Zr_xCl_6$ ($0 \leqslant x \leqslant 0.5$)." *Chem. Mater.*, **33**, 4773 (2021).
16. Y. Tomita, H. Matsushita, Y. Maeda, K. Kobayashi, and K. Yamada, "Synthesis of $Li_{3+x}In_{1-x}M_xBr_6$ (M=Zn, Co, Fe) by Nano-grinding and their ionic conductivity." *Trans. Mater. Res. Soc. Jpn.*, **33**, 973 (2008).
17. Y. Tomita, H. Matsushita, K. Kobayashi, Y. Maeda, and K. Yamada, "Substitution effect of ionic conductivity in lithium ion conductor, $Li_3InBr_{6-x}Cl_x$." *Solid State Ionics*, **179**, 867 (2008).
18. Z. Liu, S. Ma, J. Liu, S. Xiong, Y. Ma, and H. Chen, "High Ionic Conductivity Achieved in $Li_3Y(Br_3Cl_3)$ Mixed Halide Solid Electrolyte via Promoted Diffusion Pathways and Enhanced Grain Boundary." *ACS Energy Lett.*, **6**, 298 (2021).
19. X. Li, J. Liang, X. Yang, K. R. Adair, C. Wang, F. Zhao, and X. Sun, "Progress and perspectives on halide lithium conductors for all-solid-state lithium batteries." *Energy Environ. Sci.*, **13**, 1429 (2020).
20. J. Liang, X. Li, K. R. Adair, and X. Sun, "Metal Halide Superionic Conductors for All-Solid-State Batteries." *Acc. Chem. Res.*, **54**, 1023 (2021).
21. J. B. Goodenough, "Oxide-ion electrolytes." *Annu. Rev. Mater. Res.*, **33**, 91 (2003).
22. J. C. Bachman et al., "Inorganic Solid-State Electrolytes for Lithium Batteries: Mechanisms and Properties Governing Ion Conduction." *Chem. Rev.*, **116**, 140 (2016).
23. T. Famprikis, P. Canepa, J. A. Dawson, M. S. Islam, and C. Masquelier, "Fundamentals of inorganic solid-state electrolytes for batteries." *Nat. Mater.*, **18**, 1278 (2019).
24. K. Kim, D. Park, H. G. Jung, K. Y. Chung, J. H. Shim, B. C. Wood, and S. Yu, "Material Design Strategy for Halide Solid Electrolytes Li_3MX_6 (X = Cl, Br, and I) for All-Solid-State High-Voltage Li-Ion Batteries." *Chem. Mater.*, **33**, 3669 (2021).
25. A. K. Tyagi and J. Köhler, "Preparation and rietveld refinement of the structure of β-Li_3AlF_6." *Mat. Res. Bull.*, **32**, 1683 (1997).
26. Y. Yu, Z. Wang, and G. Shao, "Formulation of Li-metal-halide (LMX) solid state electrolytes through extensive first principles modelling." *J. Mater. Chem. A*, **9**, 25585 (2021).
27. A. K. Tyagi, J. Köhler, P. Balog, and J. Weber, "Syntheses and structures of Li_3ScF_6 and high pressure $LiScF_4$., luminescence properties of $LiScF_4$, a new phase in the system LiF-ScF_3." *J. Solid State Chem.*, **178**, 2620 (2005).
28. A. Bohnsack, G. Balzer, M. S. Wickleder, H.-U. Güdel, and G. Meyer, "Ternary Halides of the A_3MX_6 Type. VII. The Bromides Li_3MBr_6 (M = Sm-Lu, Y): Synthesis, Crystal Structure, and Ionic Mobility." *Z. Anorg. Allg. Chem.*, **623**, 1352 (1997).
29. J. Liang et al., "Site-Occupation-Tuned Superionic Li_xScCl_{3+x} Halide Solid Electrolytes for All-Solid-State Batteries." *J. Am. Chem. Soc.*, **142**, 7012 (2020).
30. R. A. Bhoyar, A. C. Nayak, P. K. Tawalare, S. P. Wankhede, and S. V. Moharil, "Luminescence in Li_3ScBr_6:Ce." *J. Phys. Conf. Ser.*, **1913**, 012036 (2021).
31. Z. Xu, X. Chen, K. Liu, R. Chen, X. Zeng, and H. Zhu, "Influence of Anion Charge on Li Ion Diffusion in a New Solid-State Electrolyte, Li_3LaI_6." *Chem. Mater.*, **31**, 7425 (2019).
32. M. Hamadène, F. Balegroune, A. Guehria-Laïdoudi, J. Grannec, and J. Ravez, "α-Li_3InF_6, a ternary fluoride with a new structure type." *J. Chem. Crystallogr.*, **36**, 1 (2006).
33. M. O. Schmidt, M. S. Wickleder, and G. Meyer, "Ternary Halides of the A_3MX_6 Type. VIII. On the Crystal Structure of Li_3InCl_6." *Z. Anorg. Allg. Chem.*, **625**, 539 (1999).
34. Y. Tomita, A. Fuji-I, H. Ohki, K. Yamada, and T. Okuda, "New lithium ion conductor Li_3InBr_6 studied by ^{7}Li NMR." *Chem. Lett.*, **27**, 223 (1998).
35. A. Bohnsack, F. Stenzel, A. Zajonc, G. Balzer, M. S. Wickleder, and G. Meyer, "Ternary Halides of the A_3MX_6 Type. VI. Ternary Chlorides of the Rare-Earth Elements with Lithium, Li_3MCl_6 (M = Tb-Lu, Y, Sc): Synthesis, Crystal Structures, and Ionic Motion." *Z. Anorg. Allg. Chem.*, **623**, 1067 (1997).
36. R. Schlem, T. Bernges, C. Li, M. A. Kraft, N. Minafra, and W. G. Zeier, "Lattice Dynamical Approach for Finding the Lithium Superionic Conductor Li_3ErI_6." *ACS Appl. Energy Mater.*, **3**, 3684 (2020).
37. R. Schlem, A. Banik, S. Ohno, E. Suard, and W. G. Zeier, "Insights into the Lithium Sub-structure of Superionic Conductors Li_3YCl_6 and Li_3YBr_6." *Chem. Mater.*, **33**, 327 (2021).

38. F. C. Hawthorne and R. B. Ferguson, "Refinement of the crystal structure of cryolite." *Can. Miner.*, **13**, 377 (1975).
39. A. Bohnsack and G. Meyer, "Ternary halides of the A_3MX_6 Type. IV. Ternary Halides of Scandium with Sodium, Na_3ScX_6 (X = F, Cl, Br): Synthesis, Structures, Ionic Conductivity." *Z. Anorg. Allg. Chem.*, **622**, 173 (1996).
40. F. He, E. Song, Y. Zhou, H. Ming, Z. Chen, J. Wu, P. Shao, X. Yang, Z. Xia, and Q. Zhang, "A General Ammonium Salt Assisted Synthesis Strategy for Cr^{3+}-Doped Hexafluorides with Highly Efficient Near Infrared Emissions." *Adv. Funct. Mater.*, **31**, 2103743 (2021).
41. K. Yamada, K. Kumano, and T. Okuda, "Conduction path of the sodium ion in Na_3InCl_6 studied by X-ray diffraction and ^{23}Na and ^{115}In NMR." *Solid State Ionics*, **176**, 823 (2005).
42. D. Büchel and H. J. Seifert, "Interaction of thulium, ytterbium(III) and lutetium chlorides with sodium chloride." *J. Therm. Anal. Calorim.*, **57**, 203 (1999).
43. M. S. Wickleder and G. Meyer, "Ternary Halides of the A_3MX_6 Type. III Synthesis, Structures, and Ionic Conductivity of the Halides Na_3MX_6 (X = Cl, Br)." *Z. Anorg. Allg. Chem.*, **621**, 457 (1995).
44. W. Liao and R. Dronskowski, "Trisodium yttrium(III) hexachloride." *Acta. Crystallogr. E*, **60**, 72 (2004).
45. H. Huang, H.-H. Wu, C. Chi, Y. Yang, J. Zheng, B. Huang, and S. Wang, "Phase-structure-dependent Na ion transport in yttrium-iodide sodium superionic conductor Na_3YI_6." *J. Mater. Chem. A*, **9**, 26256 (2021).
46. S. Wang, Q. Bai, A. M. Nolan, Y. Liu, S. Gong, Q. Sun, and Y. Mo, "Lithium Chlorides and Bromides as Promising Solid-State Chemistries for Fast Ion Conductors with Good Electrochemical Stability." *Angew. Chem. Int. Ed.*, **58**, 8039 (2019).
47. S. Lany and A. Zunger, "Accurate prediction of defect properties in density functional supercell calculations." *Model. Simul. Mater. Sci. Eng.*, **17**, 084002 (2009).
48. P. Gorai, H. Long, E. Jones, S. Santhanagopalan, and V. Stevanović, "Defect chemistry of disordered solid-state electrolyte $Li_{10}GeP_2S_{12}$." *J. Mater. Chem. A*, **8**, 3851 (2020).
49. M. Y. Toriyama, J. Qu, G. J. Snyder, and P. Gorai, "Defect Chemistry and Doping of BiCuSeO." *J. Mater. Chem. A*, **9**, 20685 (2021).
50. J. Liang, X. Li, K. R. Adair, and X. Sun, "Metal halide superionic conductors for all-solid-state batteries." *Acc. Chem. Res.*, **54**, 2 (2021).
51. S. A. Cotton and F. A. Hart, *The Heavy Transition Elements* (Springer, Berlin) (1975).
52. R. C. Fay, "Zirconium and Hafnium." *Coord. Chem. Rev.*, **37**, 41 (1981).
53. R. D. Shannon, "Revised effective ionic radii and systematic studies of interatomic distances in halides and chalcogenides." *Acta Crystallogr. A*, **32**, 751 (1976).
54. K. H. Park, K. Kaup, A. Assoud, Q. Zhang, X. Wu, and L. F. Nazar, "High-Voltage Superionic Halide Solid Electrolytes for All-Solid-State Li-Ion Batteries." *ACS Energy Lett.*, **5**, 533 (2020).
55. K. Wang et al., "A cost-effective and humidity-tolerant chloride solid electrolyte for lithium batteries." *Nat. Commun.*, **12** (2021).
56. H. Kwak et al., "New Cost-Effective Halide Solid Electrolytes for All-Solid-State Batteries: Mechanochemically Prepared Fe^{3+}-Substituted Li_2ZrCl_6." *Adv. Energy Mater.*, **11**, 1 (2021).
57. H. Kwak, J. Lyoo, J. Park, Y. Han, R. Asakura, A. Remhof, C. Battaglia, H. Kim, S. T. Hong, and Y. S. Jung, "Na_2ZrCl_6 enabling highly stable 3 V all-solid-state Na-ion batteries." *Energy Storage Mater.*, **37**, 47 (2021).
58. T. H. Wan and F. Ciucci, "Ab Initio Study of the Defect Chemistry and Substitutional Strategies for Highly Conductive Li_3YX_6 (X = F, Cl, Br, and I) Electrolyte for the Application of Solid-State Batteries." *ACS Appl. Energy Mater.*, **4**, 7930 (2021).
59. Y. Tomita, H. Yonekura, Y. Yamauchi, K. Kobayashi, and K. Yamada, "Substitution Effect in the Ion Conductor Li_3InBr_6, Studied by Nuclear Magnetic Resonance." *Z. Naturforsch. A*, **57**, 447 (2002).
60. Y. Tomita, H. Matsushita, H. Yonekura, Y. Yamauchi, K. Yamada, and K. Kobayashi, "Li ion conductivity of solid electrolyte, $Li_{3-2x}M_xInBr_6$ (M = Mg, Ca, Sr, Ba)." *Solid State Ionics*, **174**, 35 (2004).
61. K. Hikima, N. H. Huy Phuc, H. Tsukasaki, S. Mori, H. Muto, and A. Matsuda, "High ionic conductivity of multivalent cation doped Li_6PS_5Cl solid electrolytes synthesized by mechanical milling." *RSC Adv.*, **10**, 22304 (2020).
62. P. Adeli, J. D. Bazak, G. R. Goward, and L. F. Nazar, "Influence of Aliovalent Cation Substitution and Mechanical Compression on Li-Ion Conductivity and Diffusivity in Argyrodite Solid Electrolytes." *Chem. Mater.*, **33**, 146 (2021).
63. M. A. Kraft, S. P. Culver, M. Calderon, F. Böcher, T. Krauskopf, A. Senyshyn, C. Dietrich, A. Zevalkink, J. Janek, and W. G. Zeier, "Influence of Lattice Polarizability on the Ionic Conductivity in the Lithium Superionic Argyrodites Li_6PS_5X (X = Cl, Br, I)." *J. Am. Chem. Soc.*, **139**, 10909 (2017).
64. J. Gamon, M. S. Dyer, B. B. Duff, A. Vasylenko, L. M. Daniels, M. Zanella, M. W. Gaultois, Frédéric Blanc, J. B. Claridge, and M. J. Rosseinsky, "$Li_{4.3}AlS_{3.3}Cl_{0.7}$: A Sulfide-Chloride Lithium Ion Conductor with Highly Disordered Structure and Increased Conductivity." *Chem. Mater.*, **33**, 8733 (2021).
65. M. Yamagishi, S. Tachibana, T. Shimizu, K. Mitsuhara, and Y. Orikasa, "Analyzing Sulfur-doped Li_3InCl_6 Solid Electrolytes by X-ray Absorption Spectroscopy." *Mem. SR Cent. Ritsumeikan Univ.*, **23**, 19 (2021).
66. A. Gautam et al., "Rapid Crystallization and Kinetic Freezing of Site-Disorder in the Lithium Superionic Argyrodite Li_6PS_5Br." *Chem. Mater.*, **31**, 10178 (2019).
67. K. Wakamura, "Roles of phonon amplitude and low-energy optical phonons on superionic conduction." *Phys. Rev. B*, **56**, 11593 (1997).
68. S. Muy et al., "Tuning mobility and stability of lithium ion conductors based on lattice dynamics." *Energy Environ. Sci.*, **11**, 850 (2018).
69. D. Park, H. Park, Y. Lee, S. O. Kim, H. G. Jung, K. Y. Chung, J. H. Shim, and S. Yu, "Theoretical design of lithium chloride superionic conductors for all-solid-state high-voltage lithium-ion batteries." *ACS Appl. Mater. Interfaces*, **12**, 34806 (2020).
70. Y. Liu, S. Wang, A. M. Nolan, C. Ling, and Y. Mo, "Tailoring the cation lattice for chloride lithium-ion conductors." *Adv. Energy Mater.*, **10**, 2002356 (2020).
71. L. M. Foster, M. P. Anderson, G. V. Chandrashekhar, G. Burns, and R. B. Bradford, "The mixed alkali effect in (K, Na)-β-gallate fast ion conductor." *J. Chem. Phys.*, **75**, 2412 (1981).
72. J. L. Briant and G. C. Farrington, "Ionic Conductivity in Lithium and Lithium-Sodium Beta Alumina." *J. Electrochem. Soc.*, **128**, 1830 (1981).
73. H. Harder, A. Bunde, and W. Dieterich, "Percolation model for mixed alkali effects in solid ionic conductors." *J. Chem. Phys.*, **85**, 4123 (1986).
74. C. Reber, H. U. Güdel, G. Meyer, T. Schleid, and C. A. Daul, "Optical Spectroscopic and Structural Properties of V^{3+}-Doped Fluoride, Chloride, and Bromide Elpasolite Lattices." *Inorg. Chem.*, **28**, 3249 (1989).
75. Y. Tomita, H. Nishiyama, K. Kobayashi, Y. Kohno, Y. Maeda, and K. Yamada, "Substitution Effect for Br on the Lithium Ion Conductivity of Lithium Indium Bromide." *ECS Trans.*, **16**, 137 (2019).
76. Koji Yamada, Keiji Kumano, and Tsutomu Okuda, "Lithium superionic conductors Li_3InBr_6 and $LiInBr_4$ studied by ^7Li, ^{115}In NMR." *Solid State Ionics*, **177**, 1691 (2006).
77. A. Zevgolis, B. C. Wood, Z. Mehmedović, A. T. Hall, T. C. Alves, and N. Adelstein, "Alloying effects on superionic conductivity in lithium indium halides for all-solid-state batteries." *APL Mater.*, **6**, 047903 (2018).
78. K. Wakamura, "Correlation between high ionic conductivity and anomaly of dielectric property." *Solid State Commun.*, **86**, 503 (1993).
79. K. Wakamura, "Origin of the low-energy mode in superionic conductors." *Phys. Rev. B*, **59**, 3560 (1999).
80. C. Monroe and J. Newman, "The Impact of Elastic Deformation on Deposition Kinetics at Lithium/Polymer Interfaces." *J. Electrochem. Soc.*, **152**, A396 (2005).
81. T. Binninger, A. Marcolongo, M. Mottet, V. Weber, and T. Laino, "Comparison of computational methods for the electrochemical stability window of solid-state electrolyte materials." *J. Mater. Chem. A*, **8**, 1347 (2020).
82. A. Banik, Y. Liu, S. Ohno, Y. Rudel, A. Jiménez-solano, A. Gloskovskii, N. M. Vargas-Barbosa, Y. Mo, and W. G. Zeier, "Can substitutions affect the oxidative stability of lithium argyrodite solid electrolytes?" *ACS Appl. Energy Mater.*, **5**, 1 (2021).
83. T. Yu et al., "Superionic Fluorinated Halide Solid Electrolytes for Highly Stable Li-Metal in All-Solid-State Li Batteries." *Adv. Energy Mater.*, **11**, 2101915 (2021).
84. F. Han, A. S. Westover, J. Yue, X. Fan, F. Wang, M. Chi, D. N. Leonard, N. J. Dudney, H. Wang, and C. Wang, "High electronic conductivity as the origin of lithium dendrite formation within solid electrolytes." *Nat. Energy*, **4**, 187 (2019).
85. P. Gorai, T. Famprikis, B. Singh, V. Stevanovic, and P. Canepa, "Devil is in the defects: Electronic conductivity in solid electrolytes." *Chem. Mater.*, **33**, 7484 (2021).
86. J. O. Hill, I. G. Worsley, and L. G. Hepler, "Thermochemistry and oxidation potentials of vanadium, niobium, and tantalum." *Chem. Rev.*, **71**, 127 (1971).
87. A. G. Squires, D. O. Scanlon, and B. J. Morgan, "Native Defects and Their Doping Response in the Lithium Solid Electrolyte $Li_7La_3Zr_2O_{12}$." *Chem. Mater.*, **32**, 1876 (2020).
88. A. Squires, J. M. Dean, and B. J. Morgan, *ChemRxiv* (2021), "Aliovalent doping response and impact on ionic conductivity in the antiperovskite solid electrolyte Li_3OCl." 10.26434/chemrxiv-2021-hzrls.
89. A. Squires, D. Davies, S. Kim, D. Scanlon, A. Walsh, and B. Morgan, *ChemRxiv* (2021), "Low Electronic Conductivity of $Li_7La_3Zr_2O_{12}$ (LLZO) Solid Electrolytes from First Principles." 10.26434/chemrxiv-2021-zvwhh-v2.
90. P. Canepa, G. Sai Gautam, D. Broberg, S.-H. Bo, and G. Ceder, "Role of point defects in spinel Mg chalcogenide conductors." *Chem. Mater.*, **29**, 9657 (2017).
91. K. Sveinbjörnsson, K. Aitola, J. Zhang, M. B. Johansson, X. Zhang, J. Correa-Baena, A. Hagfeldt, G. Boschloo, and E. M. J. Johansson, "Ambient air-processed mixed-ion perovskites for high-efficiency solar cells." *J. Mater. Chem. A*, **4**, 16536 (2016).